

Building and characterization of a compact Doppler-free Rubidium frequency reference

by

Miguel Munoz Blat

Bachelor Thesis in Physics
presented to the faculty of Physics, Mathematics and Computer Science (FB
08)
at Johannes Gutenberg-Universität Mainz
7. August 2022

1st Examiner: Prof. Dr. Patrick Windpassinger

2nd Examiner: Prof. Dr. Randolph Pohl

I hereby assure that I wrote this thesis myself. I did not use any other sources than the ones indicated and quotes are referred to as such.

Mainz, August 7, 2022

Miguel Munoz Blat
AG QOQI
Institut of Physics
Staudingerweg 7
Johannes Gutenberg-Universität D-55128 Mainz
mmunozbl@students.uni-mainz.de

Table of contents

1	Introduction	1
2	Theoretical background	4
2.1	Basic scheme for Active Frequency Stabilization	4
2.2	Atomic transition frequencies of Rubidium	6
2.3	Laser Absorption Spectroscopy	7
2.4	Line broadening	8
2.4.1	Homogeneous broadening	8
2.4.2	Doppler broadening	8
2.5	Saturated Absorption Spectroscopy	11
2.5.1	Saturated Absorption in a Doppler-broadened medium	11
2.5.2	Working principle behind SAS	12
2.6	Frequency Modulation Saturated Absorption Spectroscopy	15
2.6.1	Frequency and Phase Modulation	16
2.6.2	Working principle behind the generation of the error signal	18
3	Experimental setups and results	22
3.1	Characterization of the Frequency Modulation of the light field	22
3.1.1	Phase Modulation of the light field: Electro-Optic Modulator	22
3.1.2	Setup for the characterization of the FM of the light field	24
3.1.3	Data treatment and results of the characterization of the relation modulation index versus applied voltage to the EOM	30
3.2	Investigation of the SNR dependency with the deviation frequency	35
3.2.1	Setup for Saturated Absorption Spectroscopy	36
3.2.2	Setup to generate and measure the error signal	38
3.2.3	Results of the investigation and discussion	40
4	Summary and outlook	46
5	Appendix	47
5.1	Gaussian model of the bands of the spectrum of a phase-modulated signal	47
6	Acknowledgement	50

1 Introduction

Many experiments and laser applications involving atoms require that the frequency of a continuous wave laser is stabilized onto one of their transition frequencies. For example, in laser spectroscopy of atoms and molecules the resolution of the measurements can be limited not just by the width of the spectral lines but also by the stability of the used laser. The applicability of laser spectroscopy in many fields lasts until today. For instance, in 2020, scientists at ISOLDE-CERN performed collinear laser spectroscopy on the $3s^23p^2P_{3/2} \rightarrow 3s^24sS_{1/2}$ atomic transition of $^{27-32}\text{Al}$ isotopes[1] to study their electromagnetic moments and changes in their mean-square radii, with the goal of describing the structure of midshell nuclei in the framework of the QCD theory.

Another example of an important application that requires stable lasers is laser cooling[2]. In this technique, atoms or molecules are cooled using precisely tunable lasers at frequencies close to their transition frequencies. This technique can be used i.e. to create Bose-Einstein Condensates (BECs). The QOOQI (Experimental Quantum Optics and Quantum Information) research group at Johannes Gutenberg-Universität Mainz is involved in the QUANTUS (Quantengase Unter Schwerelosigkeit) projects [3] supported by the German Space Agency (DLR). These projects, in collaboration with other German universities, are mainly aimed to develop quantum sensors based on cold and ultra-cold atoms. The latest QUANTUS IV-MAIUS project [4] has the main objective of generating Rubidium and Potassium Bose-Einstein Condensates and use them to perform dual-species atom-interferometry aboard a sounding rocket, hereby enabling a high-fidelity test of the weak equivalence principle. To create BECs, atoms need to be cooled to temperatures close to the absolute zero, which can only be achieved using highly stable lasers.

In these kind of collaborative projects between research groups of different universities it is often required to transport experimental setups and equipment from one place to another. The aim of this thesis is to address this requirement for experiments that involve stable lasers at atomic frequencies by describing the building of a compact and portable device that can be used to perform Active Frequency Stabilization of a tunable laser onto an atomic transition frequency of Rubidium and at the same time investigate which parameters in the device can be optimized to provide a better Laser Frequency Stabilization. We chose this element because it is used in the QUANTUS projects. Another reason is that this element has a relatively simple hyperfine structure of energy levels that provides atomic transitions of wavelengths ~ 780 nm which can be used to stabilize a usual 780 nm tunable diode laser.

1 Introduction

First, along Section 2 we describe all the theoretical concepts and methods that we need to consider in order to stabilize the frequency of a laser onto a transition frequency of Rubidium. Specifically, in Section 2.1 we describe the different stages in the Active Frequency Stabilization method. By doing so, we define the function the compact module that we constructed in the frequency stabilization process, which is to provide a measurement of the difference between the laser frequency and the transition frequency of Rubidium that is used as a reference to stabilize the laser. This measurement is provided in form of an electrical signal: the error signal. To generate this signal we perform Rubidium Frequency Modulation Saturated Absorption Spectroscopy method. This method combines two different techniques of Laser Spectroscopy: the Saturated Absorption Spectroscopy and the Frequency Modulation Spectroscopy. Since we perform Rubidium Laser Spectroscopy, in Section 2.2 we briefly describe the atomic structure of this element that provides the transition frequencies which we want to detect in order to generate the error signal. Then, in Section 2.3 we provide a qualitative explanation of how Laser Absorption Spectroscopy can be used to detect when a laser is tuned to one of these transition frequencies and we introduce the concept of transition lineshape, which determines the interaction of the atoms with light at different frequencies. In Section 2.4 we discuss how the broadening of the transition lineshape due to the Doppler-effect experienced by the atoms of the gas moving in the direction of the incident light affects the results of the laser spectroscopy by causing that the different transition frequencies of the hyperfine structure of Rubidium cannot be resolved. This effect is known as Doppler-broadening. To overcome this problem we use the Saturated Absorption Spectroscopy method described in Section 2.5. This technique allows us to measure a signal with resonances when the laser is tuned to the transition frequencies of Rubidium. Finally, in Section 2.6 we explain how we can obtain an error signal by modulating the frequency of the light used in the Saturated Absorption Spectroscopy method (Frequency Modulation Spectroscopy).

An important feature required in a frequency-stabilization stage is that the deviations of the laser frequency from the reference frequency onto which the laser is stabilized are measured with a high signal-to-noise ratio. This means small differences of frequency produce a high error signal. In Section 2.6.2 we derive that the signal-to-noise ratio from the error signal that we generate using the Frequency Modulation Saturated Absorption Spectroscopy method has a dependency with the deviation frequency, which is a parameter of the Frequency Modulation described in Section 2.6.1 that represents the maximum deviation of the laser frequency from its frequency when it is unmodulated. In this thesis we also investigate this dependency in order to obtain a higher signal-to-noise ratio that can result in a better Laser Frequency Stabilization. To do so, we must have control of the deviation frequency values applied to the frequency-modulated light field in the Saturated Absorption Spectroscopy method. This is the aim of Section 3.1, where we present the working principle behind the device that we use to produce the modulation of the light field: the electro-optic modulator, in

1 Introduction

3.1.1. Then, in Section 3.1.2, we present the setup used to characterize the modulation produced by the device and discuss the results in Section 3.1.3. The investigation of the dependency of the signal-to-noise ratio with the deviation frequency is then presented in Section 3.2. To do such an investigation we require to generate and measure the error signal. The setup for the generation and measurement of the error signal is presented in Sections 3.2.1 and 3.2.2. Since the setup requires generating the error signal, in Sections 3.2.1 and 3.2.2 we also detail which of the components of this setup are integrated in the compact frequency-stabilization module. Finally, the results of the investigation are presented and discussed in Section 3.2.3.

2 Theoretical background

In this section we present the theory underlying the different methods that we implement in the compact module that we constructed to perform laser frequency stabilization onto a transition frequency of Rubidium. First, we describe the function of this device in the Active Frequency Stabilization method and define what is the error signal and its importance in this method. Then we expose the fundamental concepts and methods of laser spectroscopy that we incorporate to the compact module in order to generate an error signal that can be used to stabilize a laser onto an atomic transition frequency. We also include concepts of Frequency Modulation which is used in the Frequency Modulation Spectroscopy method in order to generate an error signal of this characteristics. This concepts are later used in Section 3.1

2.1 Basic scheme for Active Frequency Stabilization

The compact frequency-stabilization module that we constructed was conceived to be used in the Active Frequency Stabilization method [5]. In this method, a feedback-loop system is used to lock a frequency-tunable laser onto a stable frequency reference (e.g. the frequency of an atomic transition) by correcting deviations of the instantaneous laser frequency from this reference frequency.

The first element of the feedback loop is the laser to be stabilized. This laser must be a frequency-tunable laser so its frequency can be adjusted to the frequency reference once a full turn in the loop is completed. Another element of the feedback loop is the frequency discriminant or discriminant. This is a device that detects the difference between the laser frequency and the frequency reference and converts it into a proportional voltage. This linear conversion of frequency differences into voltages is defined by the so called discriminant signal or error signal such that $\epsilon = D\Delta f$ is the error signal, Δf is the deviation of the laser frequency from the frequency reference and D is a constant called discriminator coefficient that characterizes this linear relation. To tightly lock the laser frequency to a reference frequency, the deviations must be detected with a high signal-to-noise ratio (SNR), this means that small frequency deviations produce electrical signals big enough to be detected and corrected. This is equivalent as having a big value of the discriminant factor D (V/Hz). The discriminant generates an error signal according to a certain discriminator coefficient that determines the signal-to-noise ratio and therefore can ultimately determine the performance of the Active Frequency Stabilization system.

2 Theoretical background

The last element of the loop is the Loop Filter, which is comprised of electronics that convert the error signal into a suitable control signal that can be fed back to the laser to correspondingly adjust its frequency towards the reference frequency. A very commonly used controller is the Proportional-Integral-Derivative controller (PID). This is a device that continuously calculates an error value as the difference between a desired setpoint, and a measured process variable –in this case the error signal– and applies a correction based on proportional, integral, and derivative terms.

One of the goals of this thesis is to describe the building of a compact discriminant that is able to generate an error signal whose reference frequency is one of the transition frequencies of Rubidium and at the same time to investigate how the SNR of this error signal can be improved to obtain a better frequency stabilization. Therefore, here we only focus in the discriminant part of the loop and do not study its performance with a Loop Filter in a frequency-stabilization feedback loop..

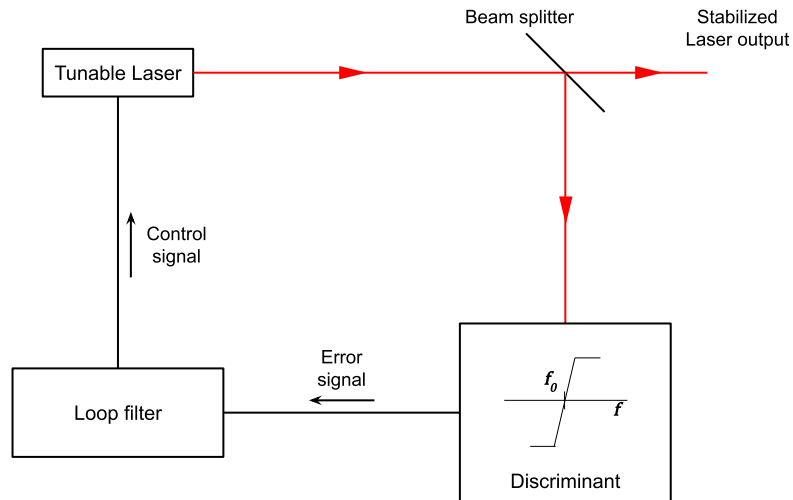


Figure 2.1: Basic scheme for Active Frequency Stabilization of a tunable laser. The laser beam is splitted using a Beam Splitter into an output beam and other beam that enters the feedback loop. The discriminant compares the frequency of the beam that enters the loop with the frequency reference and generates an error signal according to the discriminator coefficient of the device. This signal is converted by the Loop Filter into a control signal that is fed to the frequency-tunable laser to correct its frequency.

2.2 Atomic transition frequencies of Rubidium

We chose the atomic transition frequencies of Rubidium to be the frequency references of the frequency-stabilization compact module that we constructed. These transition frequencies are directly related to the atomic hyperfine structure of energy levels of Rubidium.

The nomenclature [6] used to label the energy levels of the fine structure is $n^{2S+1}L_J$, where n is the principal quantum number, S is the electron spin, L is the orbital angular momentum of the electron and J is the total angular momentum of the electron $\vec{J} = \vec{L} + \vec{S}$. To label the levels of hyperfine structure it is used the same nomenclature but also specifying in parentheses the value of total angular momentum of the atom F given by $\vec{F} = \vec{J} + \vec{I}$ where I is spin of the nucleus.

In different processes such as spontaneous emission, stimulated emission and stimulated absorption, an electron bound to the atom changes from one of these energy levels to another. The energy difference between the initial and final energy levels is called transition energy $\Delta E = E_f - E_i$, and also has an associated transition frequency, $|\Delta E| = h\nu_0$, where h is the Planck's constant and ν_0 is the transition frequency.

Rubidium is an Alkali metal and therefore is an hydrogen-like atom, in the sense that it has a weakly-bound single electron (valence electron) outside of closed shells filled with electrons. Due to this, Rubidium has a relatively simple structure of energy levels [6]. The ground state of the Rubidium's valence electron is labeled as $5^2S_{1/2}$ according to the nomenclature previously explained. The first excited states of Rb are the atomic transitions from the ground state levels $5^2S_{1/2}$ to the levels $5^2P_{1/2}$ (D1 line) and $5^2P_{3/2}$ (D2 line), showed in Figure 2.2. D2 line transitions are specially important for having wavelengths of ~ 780 nm, which is a wavelength used by many commercial lasers. In this thesis we also work with these transition frequencies, which are:

$5_2S_{1/2}(F = 2) \rightarrow 5^2P_{3/2}(F = 1, 2, 3)$ and $5^2S_{1/2}(F = 3) \rightarrow 5^2P_{3/2}(F = 2, 3, 4)$ for ^{85}Rb [8] and

$5_2S_{1/2}(F = 1) \rightarrow 5^2P_{3/2}(F = 0, 1, 2)$ and $5^2S_{1/2}(F = 2) \rightarrow 5^2P_{3/2}(F = 1, 2, 3)$ for ^{87}Rb . [9]

where ^{85}Rb (72.2%) and ^{87}Rb (27.8%) are the most abundant isotopes of Rubidium.

2 Theoretical background

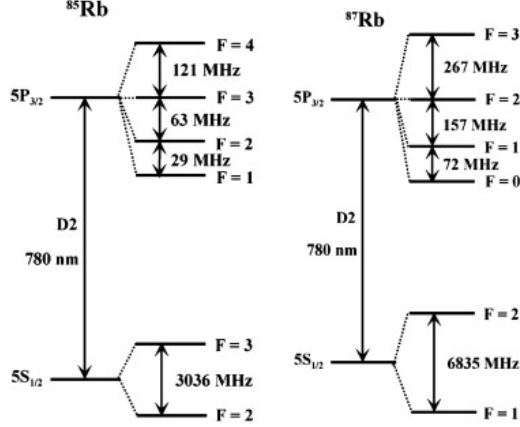


Figure 2.2: Schematic representation of the hyperfine structure of energy levels of the isotopes ^{85}Rb and ^{87}Rb and the D2 transition lines that have associated wavelengths at ~ 780 nm. Extracted from [10].

2.3 Laser Absorption Spectroscopy

To create a discriminant capable of detecting deviations of the laser frequency from a transition frequency of Rubidium we can exploit the fact that these same Rubidium atoms are resonant with light of frequency equal to one of their transition frequencies. A process that exhibits this resonance is the absorption[11], where a photon is absorbed by an atom inducing an electronic transition between two energy levels. In a cavity of volume V with n photons of frequency ν , the probability density that an atom absorbs one of these photons is

$$P_{ab} = n \frac{c}{V} \sigma(\nu) \quad (2.1)$$

where c is the speed of light and $\sigma(\nu)$ is the transition cross-section. This quantity is a function of the frequency of the incident atom ν that peaks at the transition frequency ν_0 (resonance) and characterizes the interaction of the atom with light of frequency ν . The area of the cross-section is

$$S = \int_0^{\infty} \sigma(\nu) d\nu, \quad (2.2)$$

known as the transition strength and represents the strength of the light-matter interaction. At the same time it defines a normalized lineshape function $g(\nu) = \sigma(\nu)/S$, such that $\int_0^{\infty} g(\nu) d\nu = 1$.

An example of how we can make use of the absorption to detect atomic transitions is measuring the transmission of a laser beam that passes through a Rubidium sample. If the laser frequency is close to a transition frequency of Rubidium, there is a chance

2 Theoretical background

–given by (2.2)– that the light is absorbed by the Rubidium atoms and the transmitted power through the sample decreases. The transmitted power will be minimum when the laser frequency is tuned exactly to the transition frequency, because then the transition cross-section will reach its maximum value (peak cross-section $\sigma(\nu_0)$) and the probability of absorption will be maximum. This method of detecting atomic transition frequencies implies that we perform laser absorption spectroscopy.

2.4 Line broadening

The lineshape function $g(\nu)$ was defined in the previous Section as the normalized shape of the transition cross-section $\sigma(\nu)$. Therefore, it is also a function of frequency that peaks at the transition frequency and it governs the relative magnitude of the interaction of the atom with photons over a range of frequencies. Different mechanisms lead to the broadening [12] of the lineshape function. These broadening mechanisms have an associated lineshape and the overall lineshape of the transition is given by the convolution of all them.

2.4.1 Homogeneous broadening

Homogeneous broadening mechanisms are those in which all the atoms have the same lineshapes and transition frequencies. An example is the natural or lifetime broadening, which is a consequence of the uncertainty principle that relates the lifetime of an excited state with the uncertainty of its energy and therefore of its frequency ($\Delta E = \hbar\Delta\nu = \hbar/\tau$ where τ is the lifetime of the excited state). Other common source of homogeneous line broadening are elastic collisions, which impart a phase shift to the wave function associated with the energy level and lead to a broadening $\Delta\nu = f_{col}/\pi$ where f_{col} is the collisions rate. Both mechanisms are associated with a Lorentzian profile centered in the transition frequency. The convolution of two Lorentzian functions is also a Lorentzian with a width equal to the sum of the other two

$$g(\nu) = \frac{\Delta\nu/2\pi}{(\nu - \nu_0)^2 + (\Delta\nu/2)^2}, \quad \Delta\nu = \frac{1}{2\pi} \left(\frac{1}{\tau} + \frac{2}{f_{col}} \right) \quad (2.3)$$

where $g(\nu)$ is a Lorentzian lineshape of width $\Delta\nu$

2.4.2 Doppler broadening

In contrast with the natural and collisions broadening, the Doppler broadening mechanism is a type of inhomogeneous broadening where atoms with different velocities have different transition frequencies.

To see this we can consider an atom moving with some velocity component $v_z \ll c$ (being c the speed of light) in the direction of propagation z of a monochromatic

2 Theoretical background

incident light beam of frequency ν . As a result of the Doppler effect, the frequency of the light observed by this atom is

$$\nu' = \left(1 - \frac{v_z}{c}\right)\nu \quad (2.4)$$

with $v_z > 0$ for atoms moving with velocity component in the direction of propagation of the laser beam.

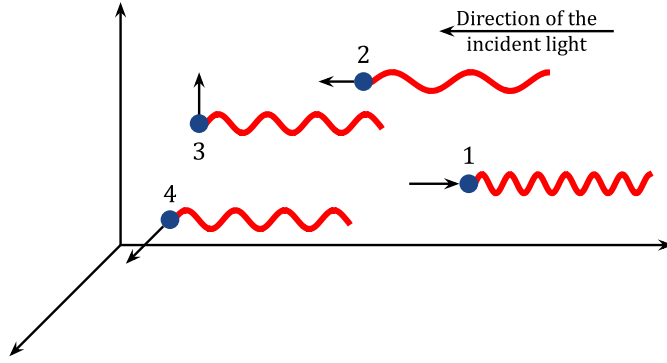


Figure 2.3: Graphic interpretation of the Doppler-frequency shift observed by atoms moving with different velocity components in the direction of the incident light. Atom 1 moves in the opposite direction of propagation of the incident light and therefore observes a higher frequency of the incident light due to Doppler effect. Atom 2 moves in the direction of propagation of light and therefore observes a lower frequency. Atoms 3 and 4 don't have any velocity component in the direction of propagation of the incident light, and don't experience any Doppler effect.

Therefore, the resonant frequency for this atoms will be given by:

$$\nu' = \nu_0 = \left(1 - \frac{v_z}{c}\right)\nu'_0 \longrightarrow \nu'_0 = \frac{\nu_0}{1 - \frac{v_z}{c}} \approx \left(1 + \frac{v_z}{c}\right)\nu_0 \quad (2.5)$$

or equivalently, when the laser is tuned to a frequency ν , it will be resonant with atoms moving with

$$v_z = \left(\frac{\nu - \nu_0}{\nu}\right)c. \quad (2.6)$$

Since the lineshapes are functions centered in the resonant frequency, they are also shifted from $g(\nu)$ to

$$g\left(\nu - \frac{v_z}{c}\nu_0\right) \equiv g_{v_z}(\nu) \quad (2.7)$$

2 Theoretical background

which means that in the medium there are atoms with different transition frequencies depending on their velocity component in the direction of the incident light v_z (inhomogeneous broadening). Typically, the atoms of the gas exhibit a Maxwellian distribution of velocities in one spatial direction (e.g. z direction), given by:

$$p(v_z) = \sqrt{\frac{M}{2\pi k_B T}} \exp\left[-\frac{Mv_z^2}{2k_B T}\right] \quad (2.8)$$

where M is the mass of the atom, k_B is the Boltzmann constant and T is the temperature. The overall inhomogeneous Doppler-broadened lineshape function $\bar{g}(\nu)$ is an average of all the lineshape functions weighted by the fraction of atoms moving with v_z (given by (2.8))

$$\bar{g}(\nu) = \langle g_{v_z}(\nu) \rangle = \int_{-\infty}^{\infty} g\left(\nu - \nu_0 \frac{v_z}{c}\right) p(v_z) dv_z. \quad (2.9)$$

This is the convolution of a Lorentzian function (assuming that $g(\nu)$ is Lorentzian) and a Gaussian function, which is the definition of the Voigt profile[13].

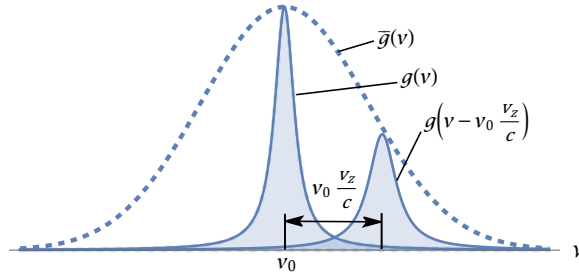


Figure 2.4: Representation of the overall lineshape function of a Doppler-broadened medium $\bar{g}(\nu)$. The overall lineshape is obtained as the average of the lineshape functions $g(\nu - \nu_0 \frac{v_z}{c})$ of atoms moving with velocity component v_z , weighted by the fraction of atoms moving with velocity v_z , given by the Maxwell-Boltzmann distribution of velocities in this direction. This weight is shown in the Figure in the form of a smaller amplitude for the lineshape $g(\nu - \nu_0 \frac{v_z}{c})$ of atoms moving $v_z \neq 0$ than the lineshape $g(\nu)$ for atoms moving with $v_z = 0$, because the Maxwellian distribution provides that the fraction of atoms to move with $v_z = 0$ is bigger than the fraction of atoms moving with $v_z \neq 0$.

The width of the Voigt profile can be estimated from the widths of the Lorentzian and Gaussian distribution as:

$$f_V \approx f_L/2 + \sqrt{f_L^2/4 + f_G^2} \quad (2.10)$$

where f_L and f_G are the FWHM of the Lorentzian and Gaussian profiles respectively. Therefore $f_V \geq f_G$. The Gaussian linewidth at room temperature is for the transition frequencies of the D2 line ($\lambda_0 \sim 780$ nm), from the Maxwellian distribution of

2 Theoretical background

velocities (2.8), $f_G = 2\sqrt{2\ln 2k_B T/M\lambda_0^2} \approx 500\text{MHz}$ while the transition frequencies of the Rubidium D2 line are spaced by 30-300 MHz[8][9]. This means that the individual lineshapes at the transition frequencies of the hyperfine structure of Rb are swallowed by a bigger lineshape from the Doppler-broadening. Therefore, the resonances at the different transition frequencies can no longer be resolved so the method that we proposed in Section 2.3 to detect when the laser is tuned to a transition frequency of Rb cannot be applied. However, there are techniques to overcome the problem of Doppler-broadening so the transition frequencies can be identified in a Doppler-broadened medium. An example is the Saturated Absorption Spectroscopy method.

2.5 Saturated Absorption Spectroscopy

A way of overcoming the Doppler broadening and therefore being able to detect the transition frequencies of Rubidium is using the method called Saturated Absorption Spectroscopy (SAS)[14]. In this technique, two counter-propagating overlapping laser beams of exactly the same frequency interact with the atoms of the gas. This technique makes use of the saturation of the absorption in the medium to produce peaks of transmitted intensity of one of the two beams through the sample when their frequency is tuned to a transition frequencies of Rb. Using this method the transition frequencies can be detected despite the Doppler broadening.

2.5.1 Saturated Absorption in a Doppler-broadened medium

The loss of intensity due to absorption after the beam has traveled a distance z in the absorbing medium [15] is given by:

$$I(z) = I(0)\exp[-\alpha z] \quad (2.11)$$

where α is the absorption coefficient. In a saturable medium, the absorption coefficient decreases with the increasing incident optical intensity (saturation).

$$\alpha(\nu) = \frac{\alpha_0(\nu)}{1 + I/I_s(\nu)}, \quad (2.12)$$

where $\alpha_0(\nu)$ is the unsaturated absorption coefficient and $I_s(\nu)$ is the saturation intensity. Both $\alpha_0(\nu)$ and $I_s(\nu)$ depend on ν since they are proportional to the transition cross-section $\sigma(\nu)$ (and hence to $g(\nu)$).

In the Doppler-broadened medium, each group of atoms moving with v_z have associated their own absorption coefficient, given by

$$\alpha_{v_z}(\nu) = \frac{\alpha_{0v_z}(\nu)}{1 + I/I_{sv_z}(\nu)} \quad (2.13)$$

2 Theoretical background

where now $\alpha_{0v_z}(\nu)$ and $I_{sv_z}(\nu)$ are proportional to $g_{v_z}(\nu)$. When a laser beam of frequency ν interacts with atoms in a Doppler-broadened medium it will produce saturation of the absorption coefficient α_{v_z} associated with atoms with velocity component $v_z = \frac{\nu - \nu_0}{\nu} c$. When the intensity is large compared to the saturation intensity $I_s(\nu) \ll I$, the absorption coefficient saturates and there is no net absorption. In an approximated model of only two atomic energy levels (ground state and excited state), this takes place when the population of atoms in the ground state is the same as the population of atoms in the excited state.

2.5.2 Working principle behind SAS

As stated before, in this technique two counterpropagating and overlapping laser beams travel through an atomic gas, which is a saturable Doppler-broadened medium, and are used to produce Doppler-free spectroscopy. One of the beams, called pump beam has typically more optical power than the other, called probe beam. When the frequency of these beams is different from the resonant frequency of the atoms ν_0 , one beam interacts with the group of atoms that move with some velocity component in z direction v_z , while the other beam, since they are counterpointing, interacts with the group of atoms moving with $-v_z$. This produces some saturation in the absorption coefficients α_{v_z} and α_{-v_z} or equivalently, in the two energy levels approximation, it produces some depopulation of the atoms in the ground state moving with v_z and $-v_z$, as represented in Figure 2.5a. However, when the frequency is tuned to the resonant frequency, both beams will address the same group of atoms, which are those moving with $v_z \approx 0$. When this happens, the strong pump beam excites this group of atoms and causes the saturation of the absorption coefficient $\alpha_{v_z=0}$. Therefore, the pump beam serves to bleach the absorptive medium leading to an increase of the transmission of the probe beam through the sample, which is reflected as a peak of its transmitted intensity when the frequency of the beams is tuned to a resonant transition frequency of the atomic gas.

2 Theoretical background

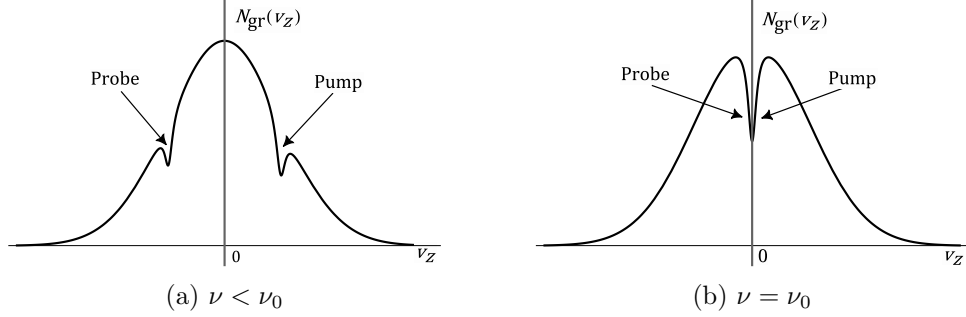


Figure 2.5: Distribution of the number of atoms in the ground state N_{gr} with velocity component v_z (a) when the frequency of the laser ν is tuned to a frequency smaller than the transition frequency ν_0 . The pump beam interacts with atom moving with $v_z = (\frac{\nu - \nu_0}{\nu})c$ and the probe beam with atoms moving with $v_z = -(\frac{\nu - \nu_0}{\nu})c$ since they are counter-propagating. (b) When the laser frequency is tuned to the resonant frequency both beam interact with the same group of atoms, those moving with $v_z \approx 0$.

Crossover frequencies

When two transitions with frequencies ν_1 and ν_2 share a ground state and differ in frequency by less than the Doppler linewidth, apart from the hyperfine structure peaks, we can also have other peaks in between, called crossover frequencies that correspond to $\nu_c = \frac{\nu_1 + \nu_2}{2}$.

To illustrate this we can imagine a situation where our laser is tuned to a frequency $\nu_1 < \nu < \nu_2$. Considering $v_z > 0$ in the direction of the probe beam and defining from (2.6) $v_{zj} = \frac{|\nu - \nu_j|}{\nu}c$ ($j = 1, 2$). The pump beam will interact with two different groups of atoms: those moving with $-v_{z1}$ and those moving with $+v_{z2}$, while the counter-propagating probe beam will address those atoms moving with $+v_{z1}$ and $-v_{z2}$. As the frequency is increased, v_{z1} increases and v_{z2} decreases. Looking at Figure 2.6a, the ground-state depopulation holes produced by the probe beam move to the left while the holes produced by the probe beam move to the right. Therefore, at some point the two holes will encounter each other, leading to the same situation described before where the pump beam excites a group of atoms and the probe beam that addresses the same group of atoms experiences an increase of its transmission through the medium. The only difference is that the pump beam and the probe beam produce excitation to different energy levels, but the effect is equivalent since the population of atoms in the ground state is depleted by the pump beam, and the probe beam finds fewer atoms in the ground state to excite, leading again to an increase of its transmission through the atomic gas. This situation occurs when $v_{z1} = v_{z2}$, condition that gives the crossover frequency:

2 Theoretical background

$$\left(\frac{\nu_c - \nu_1}{\nu_c}\right) c = \left(\frac{\nu_2 - \nu_c}{\nu_c}\right) c \longrightarrow \nu_c = \frac{\nu_1 + \nu_2}{2} \quad (2.14)$$

If we measure the transmission of the probe beam through the Rb vapor cell, at this frequency there will also be a transmission peak.

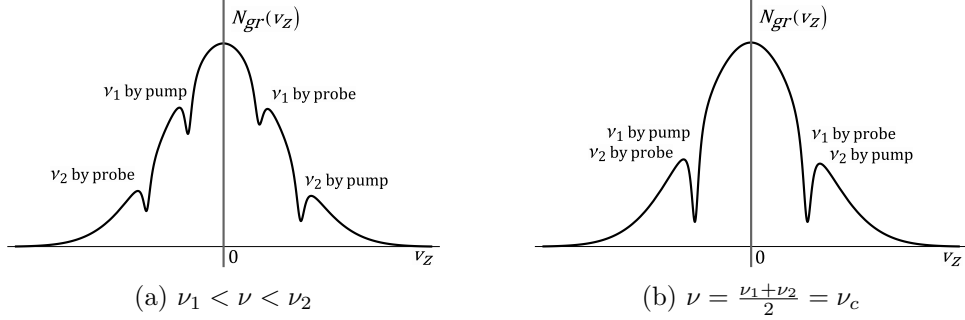


Figure 2.6: Distribution of the number of atoms in the ground state N_{gr} with velocity component v_z :

(a) When the frequency of the laser is tuned to a frequency $\nu_1 < \nu < \nu_2$ being ν_1 and ν_2 two different transition frequencies spaced by less than the width of the Maxwellian distribution of velocities. The pump beam interacts with atoms moving with $v_z = \frac{\nu_1 - \nu}{\nu} c$ and $v_z = \frac{\nu - \nu_2}{\nu} c$ while the probe beam with atoms moving with $v_z = -\frac{\nu - \nu_1}{\nu} c$ and atoms moving with $v_z = \frac{\nu_2 - \nu}{\nu} c$ because propagates in the opposite direction of the pump beam.

(b) when the laser frequency is tuned to the crossover frequency $\nu_c = \frac{\nu_1 + \nu_2}{2}$ both beams interact with atoms moving with $v_z = \pm \frac{\nu_2 - \nu_1}{\nu_1 + \nu_2} c$ producing saturation of the absorption and hence resulting in a increase of the transmission of the probe beam at this frequency.

Connecting with the purpose of using this method to construct our discriminant, this technique allows us to detect when the laser is tuned to a transition frequency due to the increase of the transmission of the probe beam through the Rubidium sample at this frequencies. The optical intensity signal of the probe beam transmitted through the sample, which we can call the 'SAS signal' $I_T(\nu)$, presents resonant peaks at the transition and crossover frequencies. The linewidth of these peaks can approach the natural width of the atomic transitions, so the different transition frequencies from the hyperfine structure energy levels can be resolved and distinguished from each other using the Saturated Absorption Spectroscopy method.

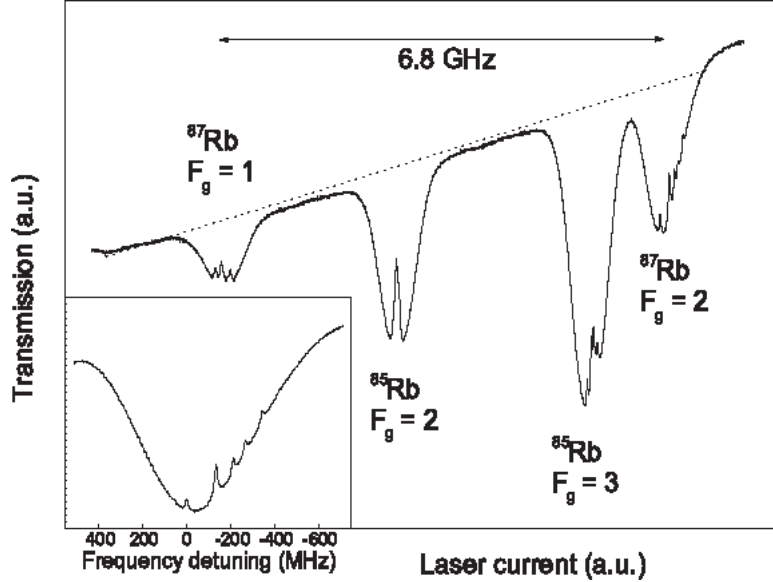


Figure 2.7: Measurement of the SAS signal extracted from [16]. The transmission of the probe beam through a Rb sample is presented as a function of the drive current of a tunable diode laser. Different values of the current correspond to different lasing wavelengths of the laser. In the picture they can be seen the Doppler-broadening profile in the decrease of the transmission and inside the Doppler-broadened profile the transmission peaks that correspond to the D2 line transition and crossover frequencies of ^{85}Rb and ^{87}Rb .

2.6 Frequency Modulation Saturated Absorption Spectroscopy

We want to construct a compact discriminant device that can be used to stabilize a tunable laser onto a transition frequency of Rb. With the SAS method described in Section 2.5 we obtain a signal $I_T(\nu)$ with narrow peaks at the different transition frequencies. However, in Section 2.1 we stated that the discriminant of a frequency-stabilization loop must provide a signal—the error signal—that is proportional to deviations of the laser frequency from a reference frequency. The SAS signal $I_T(\nu)$ does not have this characteristics, since it is resonant instead of linear at the transition frequencies that we want to use as reference in our compact discriminant. Nevertheless, this kind of signal can be obtained from the SAS signal by performing Frequency Modulation of the light field used in the SAS method. The technique of modulating the light field to perform spectroscopy is known as Frequency Modulation Spectroscopy[19]. We call Frequency Modulation Saturated Absorption Spectroscopy to the combination of this method and the Saturated Absorption Spectroscopy method (FM SAS).

2.6.1 Frequency and Phase Modulation

We can modulate the frequency of the light field used in the SAS method described in Section 2.5 in order to generate an error signal with one of the transition frequencies of Rb as frequency reference, such that the error signal is proportional to deviation of the laser frequency to this frequency reference. In general, modulation is the process of encoding information from a message source into a carrier signal. Let the carrier signal be

$$x(t) = A_c e^{i\omega_c t} \quad (2.15)$$

where ω_c is the carrier angular frequency and A_c its amplitude. Specifically, in Frequency Modulation [17] the frequency ω of the carrier wave is varied at every instant. Frequency and Phase Modulation cannot be separated from each other, since the instantaneous angular frequency and the phase are related by

$$\omega(t) = \frac{d\varphi}{dt}. \quad (2.16)$$

Hence, if the phase is modulated by a message signal $m(t)$ such that

$$\varphi(t) = \omega_c t + m(t). \quad (2.17)$$

then the modulation of the frequency, from (2.16), will be

$$\omega(t) = \omega_c + \frac{dm(t)}{dt} \quad (2.18)$$

This relation is important since in fact we perform Phase Modulation of the light field, but it can be interpreted as an equivalent Frequency Modulation that provides an instantaneous angular frequency given by (2.20).

Thereby, considering a sinusoidal message signal, the corresponding phase-modulated signal is

$$x_{PM}(t) = A_c e^{i(\omega_c t + \beta \sin \Omega t)}, \quad (2.19)$$

the instantaneous phase is given by $\varphi(t) = \omega_c t + \beta \sin \Omega t$ and the corresponding frequency, given by (2.20), is:

$$\omega(t) = \omega_c + \beta \Omega \cos \Omega t \quad (2.20)$$

where Ω is the frequency of the message signal, called modulation frequency and β is its amplitude of the message signal, called modulation index. Therefore, a sinusoidal Phase Modulation corresponds as well to sinusoidal Frequency Modulation but with a phase lag of 90° . The maximum deviation of the frequency from the carrier frequency is given by $\Delta\omega = \beta\Omega$, called frequency deviation. The sinusoidal frequency modulation of the light field is used in the method of Frequency Modulation Spectroscopy that we use in Section 2.29 to obtain the error signal with a transition frequency of Rb as frequency reference..

2 Theoretical background

The expression (2.19) can be rewritten in terms of a series of Bessel functions:

$$x_{PM}(t) = A_c e^{i\omega_c t} \left\{ J_0(\beta) + \sum_{k=1}^{\infty} J_k(\beta) e^{ik\Omega t} + \sum_{k=1}^{\infty} (-1)^k J_k(\beta) e^{-ik\Omega t} \right\} \quad (2.21)$$

where $J_k(\beta)$ are the k^{th} order Bessel functions of the first kind. This can be interpreted as an infinite set of waves that propagate with frequencies ω_c , $\omega_c \pm \Omega$, $\omega_c \pm 2\Omega, \dots$, and whose relative amplitudes are determined by the Bessel functions $J_0(\beta)$, $\pm J_1(\beta)$, $\pm J_2(\beta) \dots$, which individually carry part of the power content of the phase-modulated signal. To see this more clearly one can look at the frequencies spectrum evaluating the Fourier transform of x_{PM} . Using the fact that the Fourier transform of $e^{i\omega_0 t}$ is $\delta(\omega - \omega_0)$ it follows that

$$\mathcal{F}(x_{PM})(\omega) = A_c [J_0(\beta)\delta(\omega - \omega_c) + \sum_{k=1}^{\infty} J_k(\beta)\delta(\omega - (\omega_c + k\Omega)) + \sum_{k=1}^{\infty} (-1)^k J_k(\beta)\delta(\omega - (\omega_c - k\Omega))] \quad (2.22)$$

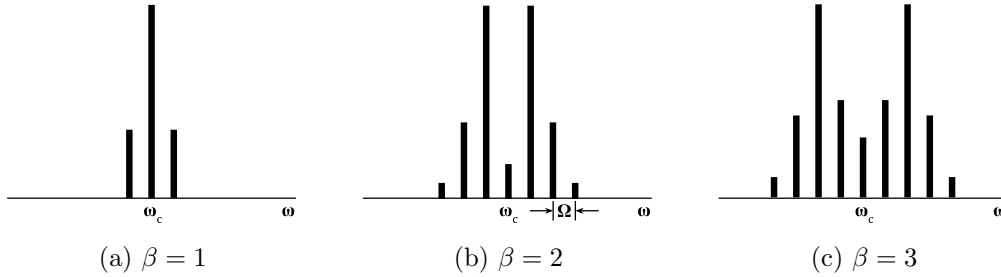


Figure 2.8: Frequency Spectrum of a phase-modulated signal for different values of the modulation index β . The relative amplitudes of the bands are given by $J_k^2(\beta)$ and represent their power content. The spectrum is symmetric respect to the carrier frequency and as the modulation index increases, more sidebands appear.

This corresponds to an infinite set of delta peaks equally spaced by an integer number of times the modulation frequency Ω . Again, the amplitude of the bands in the frequency spectrum is proportional to the Bessel functions $J_k(\beta)$ [18]. The band at the carrier frequency is called the carrier band and the rest are called sidebands i.e. bands at $\omega_c \pm \Omega$ are the first two sidebands. This nomenclature is often also used to address the waves/Fourier components oscillating with these frequencies. The spectrum of bands of a phase-modulated signal described here is relevant for the characterization of the Frequency Modulation of the light described in Section 3.1. This characterization is later used to investigate how we can optimize the laser stabilization in Section 3.2.

2 Theoretical background

2.6.2 Working principle behind the generation of the error signal

To perform Frequency Modulation of the light field implies that the temporal part of the electric light field acts now as the carrier signal discussed in Section 2.6.1. The Doppler-free spectroscopy described in Section 2.5, provides an optical intensity signal $I_T(\omega)$ with narrow peaks centered in the transition frequencies (and crossover frequencies). The sinusoidal Frequency Modulation of this signal leads to $I_T(\omega) \rightarrow I_T(\omega_c + \beta\Omega \cos \Omega t)$. If the amplitude of the sinusoidal Frequency Modulation $2\Delta\omega = 2\beta\Omega$ is smaller than the linewidth of the resonance [20], then the frequency-modulated SAS signal varies over time as:

$$I_T(\omega_c + \beta\Omega \cos \Omega t) \approx I_T(\omega_c) + \left. \frac{dI_T}{d\omega} \right|_{\omega_c} \Omega\beta \cos \Omega t. \quad (2.23)$$

this is the first order Taylor expansion of $I_T(\omega_c + \beta\Omega \cos \Omega t)$ around ω_c , valid for $\omega_c \gg \beta\Omega$ (small frequency deviation $\Delta\omega = \beta\Omega$ from the carrier frequency ω_c), which is true in our case since we use modulation frequencies of the order $\sim 10^7$ Hz and modulation indices of $\beta \sim 1$, while the optical frequency of the laser is of the order of $\sim 10^{15}$ Hz. The term $\left. \frac{dI_T}{d\omega} \right|_{\omega_c}$ from the Taylor-expanded expression (2.23) will constitute our error signal [21].

Figure 2.9 provides a graphic interpretation of how the modulation of the light frequency can lead to this expression. Considering a situation where the laser frequency (carrier frequency ω_c) is in the vicinity of a resonant peak of the SAS signal $I_T(\omega)$ and the deviation frequency $\Delta\omega$ is small compared to the linewidth of this resonance, then the sinusoidal modulation of the laser frequency leads to the periodic increase and decrease of the intensity signal $I_T(\omega)$. This periodic increase and decrease of the signal is synchronized with the periodicity of the modulation frequency that scans a small region of the resonance. Furthermore, the maximum increase or decrease of the signal is bigger when the slope of the resonance is also bigger because the difference between $I_T(\omega)$ and $I_T(\omega_C \pm \Delta\omega)$ is greater. This situation can also be described in a more quantitative way that connects with (2.23) by considering that, since the deviation frequency $\Delta\omega$ is small compared to the linewidth of the resonant peak, we can approximate the lineshape of the signal $I_T(\omega)$ to an straight line in the region $\omega_c \pm \Delta\omega$. A concept that connects to the linear approximation of a function is the first order Taylor expansion, which we can evaluate in this case around the center point ω_c of the approximation region, giving

$$I_T(\omega) \approx I_T(\omega_c) + \left. \frac{dI_T}{d\omega} \right|_{\omega_c} (\omega - \omega_c) \quad (2.24)$$

which is the equation of a straight line tangent to the function $I_T(\omega)$ at ω_c . Now if we consider the modulation of the frequency $\omega(t) = \omega_c + \beta\Omega \cos \Omega t$ it leads to the same expression (2.23), where the the term $\cos \Omega t$ describes how the intensity signal varies synchronously with the instantaneous frequency $\omega(t)$ and the maximum deviation of the signal $I_T(\omega(t))$ from its value in absence of modulation (at ω_c) is given by the

2 Theoretical background

derivative $\frac{dI_T}{d\omega}$ at ω_c , as we qualitatively exposed before through the concept of the slope of the function.

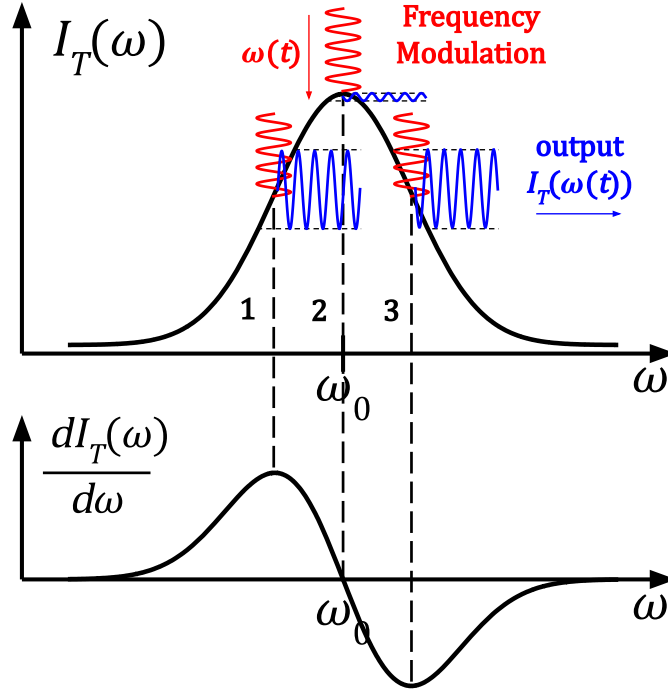


Figure 2.9: Graphic interpretation of the effect of the frequency modulation of the light field in the SAS method when the deviation frequency is smaller than the linewidth of a resonance of the signal $I_T(\omega)$. The sinusoidal variation over time of the light frequency, shown in red in the Figure, leads to a synchronized and also sinusoidal variation of the signal $I_T(\omega)$ from its value when there is no modulation (at the carrier frequency ω_c), shown in blue in the Figure. The amplitude of the sinusoidal variation of the SAS signal from its value at a given ω_c is proportional to the derivative of the SAS signal at that frequency, shown in a graph below. Thus, in 1 the derivative is maximum so it is the amplitude of the sinusoidal variation while in 2, the resonance, the derivative is 0, leading to almost no variation with time of the SAS signal from its value at the resonance $I_T(\omega_0)$. For $\omega_c > \omega_0$ the derivative is negative, which results in a 180° phase shift of the sinusoidal variation respect to 1 and the magnitude of the derivative is again maximum.

To see that the term $\frac{dI_T}{d\omega}$ satisfies the conditions to be considered as an error signal like the one that we described in Section 2.1 we can consider a resonant peak of the SAS signal $I_T(\omega)$ and approximate this resonance to a Lorentzian lineshape. If we

2 Theoretical background

look at the derivative of a Lorentzian with peak value I_0 and width Γ centered in the resonance frequency ω_0 :

$$I_T(\omega) \approx L(\omega) = \frac{I_0}{1 + \left(\frac{\omega - \omega_0}{\Gamma/2}\right)^2} \quad \frac{dL}{d\omega} = \frac{-I_0 2(\omega - \omega_0)/(\Gamma/2)^2}{\left[1 + \left(\frac{\omega - \omega_0}{\Gamma/2}\right)^2\right]^2} \quad (2.25)$$

and for small deviations from the resonant frequency $\omega \approx \omega_0$

$$\frac{dL}{d\omega} \approx \frac{2I_0}{(\Gamma/2)^2}(\omega_0 - \omega) \quad \text{for} \quad \omega \approx \omega_0. \quad (2.26)$$

it follows that the relation between the frequency and the derivative is approximately linear, which is the condition that we required for the error signal in Section 2.1. Furthermore, deviations of the laser frequency towards frequencies bigger than the resonant frequency lead to negative values of the signal and vice versa, while at the resonant frequency the derivative is zero.

The optical signal $I_T(\omega + \beta\Omega \cos \Omega t)$ can be converted into an electrical signal by measuring it with a photodetector. Now, to obtain a DC error signal that can be assimilated by the Loop Filter the derivative term $\left. \frac{dI_T}{d\omega} \right|_{\omega_c} \Omega\beta \cos \Omega t$, which is an AC term, must be demodulated. This can be done electronically by using a mixer and a low-pass filter. The mixer is a device that provides as an output the product of two input signals. Therefore, by feeding the mixer with the frequency-modulated intensity signal and a RF sinusoidal signal $\cos \Omega t$, which can be provided by a function generator, we obtain the output:

$$I_T(\omega_c + \beta\Omega \cos \Omega t) \cos \Omega t = I_T(\omega_c) \cos \Omega t + \Omega\beta \left. \frac{dI_T}{d\omega} \right|_{\omega_c} \cos^2 2\Omega t \quad (2.27)$$

and using the trigonometric relation $\cos a \cos b = \frac{1}{2}[\cos(a+b) + \cos(a-b)]$ it follows

$$I_T(\omega_c + \beta\Omega \cos \Omega t) \cos \Omega t = I_T(\omega_c) \cos \Omega t + \frac{1}{2}\Omega\beta \left. \frac{dI_T}{d\omega} \right|_{\omega_c} [1 + \cos 2\Omega t] \quad (2.28)$$

where there is a DC term proportional to the derivative of the spectral feature. The rest of the terms oscillate with Ω and 2Ω and can be suppressed using a low-pass-filter, leaving only the term

$$\epsilon = \frac{1}{2}\Omega\beta \left. \frac{dI_T}{d\omega} \right|_{\omega_c} \approx \frac{1}{2}\Omega\beta \frac{2I_0}{(\Gamma/2)^2}(\omega_0 - \omega_c) \quad \text{for} \quad \omega_c \approx \omega_0. \quad (2.29)$$

which is the error signal.

2 Theoretical background

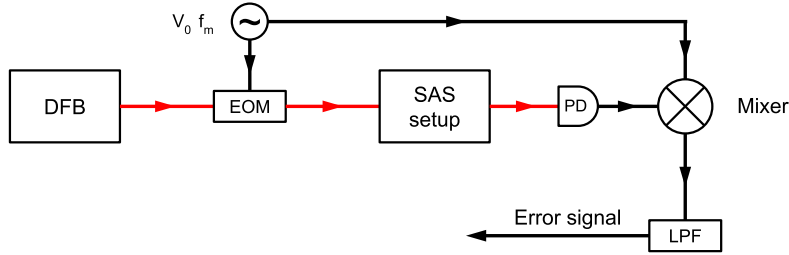


Figure 2.10: Scheme for obtaining a DC error signal with one of the transition frequencies of Rubidium as a lock point. the beam output of a DFB tunable laser undergoes Frequency Modulation by the EOM, voltage-controlled by a function generator with a modulation frequency f_m . The optical signal after passing through the spectroscopy setup $I_T(\omega + \beta\Omega \cos \Omega t)$, is measured by a photodetector (PD) and is demodulated by the mixer and the low-pass filter (LPF) to obtain a DC error signal.

As mentioned in Section 2.1, a very important feature in frequency stabilization is the signal-to-noise ratio (SNR) of the error signal. This is the response of the discriminant in form of a voltage when there are small deviations of the laser frequency from the reference frequency. With the method previously described we obtain the error signal as a signal proportional to the derivative of a resonant lineshape. This derivative presents in general a linear regime near the resonant frequency as it can be seen in expression (2.26) and in Figure 2.11 (considering the resonance as a Lorentzian). The error signal is proportional to this derivative and the corresponding discriminator factor is given by (2.29). This expression predicts that the discriminator coefficient and therefore the SNR can be enhanced by increasing the deviation frequency $\Delta\omega = \beta\Omega$. In Section 3.2 we investigate this dependency of the slope of the error signal with the deviation frequency.

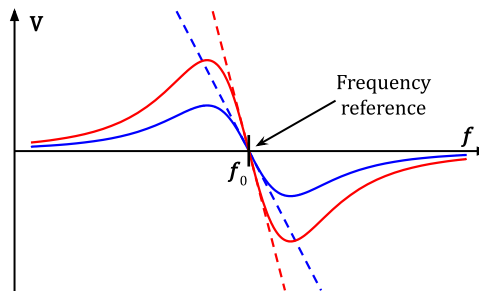


Figure 2.11: Derivative of a Lorentzian as an error signal. There are presented together two error signals with different amplitudes: the red signal has bigger amplitudes than the blue signal and therefore its slope, indicated with the dashed line, is also bigger (bigger signal-to-noise ratio).

3 Experimental setups and results

In this Section we describe the different setups used to put into practice the methods explained in Section 2 and how they are implemented in the compact discriminant module. We also describe the setup and method used to characterize the frequency modulation of the light field. We use this characterization in the investigation of the dependency of the SNR of the error signal with the deviation frequency as discussed in the previous section. We also include the setup used for this investigation, that requires measuring directly the error signal provided by the discriminant setup. At the same time, we present and discuss the results obtained for the FM characterization and the research of the SNR dependency with the modulation of the light in the Frequency Modulation Saturated Absorption Spectroscopy method.

3.1 Characterization of the Frequency Modulation of the light field

As discussed in section 2.6.2, we sinusoidally modulate the frequency of the light field used to perform Saturated Absorption Spectroscopy in order to generate an error signal in which the frequency reference is an atomic transition frequency of Rubidium. Expression 2.26 predicts that the signal-to-noise ratio (SNR) provided by this error signal is proportional to the amplitude of the sinusoidal Frequency Modulation applied to the light field, called deviation frequency. We want to investigate the relation of the SNR with the deviation frequency because higher SNR can provide a better frequency stabilization. To do such an investigation we first must have control of the deviation frequency. This requires to understand how the light field is modulated in practice: using an Electro-Optic Modulator (EOM). This device produces a sinusoidal Phase Modulation that from relation (2.16) we know that results in an also sinusoidal Frequency Modulation. The frequency deviation $\Delta\omega$ is related to the modulation index β and the modulation frequency Ω of the Phase Modulation by $\Delta\omega = \beta\Omega$, as stated in Section 2.6.1. Therefore, the aim of this Section is to control the values of the modulation index and modulation frequency produced by the EOM in order to have control of the deviation frequency.

3.1.1 Phase Modulation of the light field: Electro-Optic Modulator

To produce Phase Modulation of a laser light field we use an electro-optic modulator (EOM). To control the values of the modulation index and the modulation frequency of the Phase Modulation we first must understand the working principle behind the

3 Experimental setups and results

EOM[22], which is based on the electro-optic effect.

The electro-optic effect is the dependency of the refractive index of some materials with the electric field. In particular, in the Pockels electro-optic effect, the electro-optic material shows a linear dependency of its refractive index with the applied electric field:

$$n(E) \approx n - \frac{1}{2}rn^3E \quad (3.1)$$

where n is the refractive index in absence of applied field, E is the magnitude of the applied electric field and r is the Pockels coefficient. This coefficient is characteristic of the electro-optic material and since these are usually anisotropic crystals the coefficient is different depending on the direction of propagation of the light and the direction of the applied electric field.

An electro-optic modulator is a Pockels cell, this is essentially an electro-optic crystal placed between two metal plane plates that work as electrodes to which a potential V is applied in order to create an electric field E . The phase shift induced to a light field that passes through a Pockels cell of length L is

$$\varphi = n(E)kL = \varphi_0 - \pi \frac{rn^3EL}{\lambda} \quad (3.2)$$

where $\varphi_0 = 3\pi nL/\lambda$, and λ is the free-space wavelength. Using that $E = V/d$ (d is the separation between the electrodes):

$$\varphi = n(E)kL = \varphi_0 - \pi \frac{V}{V_\pi} \quad (3.3)$$

where $V_\pi = \frac{d}{L} \frac{\lambda}{\pi rn^3}$ is the half-wave voltage (applied voltage at which the phase shift is π). Therefore, applying a sinusoidal potential $V(t) = V_0 \sin \Omega t$ to the plates (e.g. using a function generator), Phase Modulation can be produced:

$$\varphi = n(E)kL = \varphi_0 - \pi \frac{V_0}{V_\pi} \sin \Omega t \quad (3.4)$$

and thereby, comparing with the sinusoidal phase modulation described in Section 2.6.1, the modulation index is given by

$$\beta = \pi \frac{V_0}{V_\pi}. \quad (3.5)$$

Hence, the EOM can produce sinusoidal Phase Modulation of the laser light field, that from expression (2.20) we know that is equivalent to an also sinusoidal Frequency Modulation. The angular modulation frequency Ω of the FM is known since it is set externally by the function generator that drives the EOM. On the other hand, the modulation index β is proportional to the amplitude of the sinusoidal voltage applied to the EOM. Therefore, to have control of the value of the modulation index

3 Experimental setups and results

we must characterize this relation, which requires finding the value of the parameter $\frac{\pi}{V_\pi}$. Relation (3.5) does not predict any dependency of the modulation index with the modulation frequency f_m . In practice, the V_π parameter and therefore the modulation index will depend slightly on the modulation frequency. According to the company iXblue, that supplied the NIR-MPX800-LN-0.1 EOM that we use, the dependency with f_m of the half-wave voltage for light of 780 nm wavelength is:

$$V_\pi(f_m) \approx (1 + 2.76 \times 10^{-9} f_m) \times 1.54 \quad V, \quad (3.6)$$

for modulation frequencies f_m below the electro-optical bandwidth of the EOM ($f_m < 150$ MHz). From 3.5, the predicted dependency of the modulation index with f_m is

$$\beta(V_0, f_m) = \frac{\pi V_0}{(1 + 2.76 \times 10^{-6} f_m) \times 1.54} \quad (3.7)$$

Nevertheless, the supplier company iXblue warns that even though the relation was derived making use of data from the device, this calculation is theoretical and extrapolated from a measurement at $f_m=50$ kHz, so it must be taken only as guideline. For this reason, we characterize the relation of the modulation index and the applied voltage at different modulation frequencies that we use in the investigation of the SNR.

3.1.2 Setup for the characterization of the FM of the light field

To characterize the relation between the modulation index and applied voltage to the EOM we can make use of one of the features of a sinusoidally phase-modulated signal described in Section 2.6.1, which is that its frequency spectrum consists of a series of bands (Fourier components with frequencies $\omega_c, \omega_c \pm \Omega, \omega_c \pm 2\Omega, \dots$) whose relative amplitude depend on the modulation index. Therefore, we want to construct a setup to obtain a measurement of the frequency spectrum of a phase-modulated signal, because then we can extract the value of the modulation index from the relative amplitude of the bands. To measure directly the frequency spectrum would require that we are able to detect the optical frequencies of the modulated field. However, response time of photodetectors ($\sim 10^{-11}$ s) is not small enough to measure oscillations of an optical field ($\sim 10^{-15}$ s). For this reason, we make use of the so-called 'beat signal'[23].

We consider two monochromatic linearly polarized light beams \vec{E}_1 and \vec{E}_2 oscillating at optical frequencies ω_1 and ω_2 such that

$$\vec{E}_j = \vec{e}_j E_j \cos(\vec{k}_j \vec{r} - \omega_j t + \varphi_j), \quad j = 1, 2 \quad (3.8)$$

where \vec{e}_j is the polarization vector of the field j , E_j its amplitude and \vec{k}_j its wavevector. Their optical power is given by $P_j = \frac{1}{2} \epsilon_0 c E_j^2 A_{eff}$ being A_{eff} the effective area perpendicular to the direction of propagation of the light beam, c the speed of light and ϵ_0 the vacuum permittivity.

3 Experimental setups and results

If these fields are superimposed in a photodetector. The photocurrent measured by the detector $i(t)$ exhibits a term oscillating at $|\omega_1 - \omega_2|$, which is the 'beat signal'

$$i(t) = R_\lambda \left\{ P_1 + P_2 + \vec{e}_1 \vec{e}_2 \sqrt{P_1 P_2} \cos [(\vec{k}_1 - \vec{k}_2) \vec{r} - (\omega_1 - \omega_2)t + (\varphi_1 - \varphi_2)] \right\} \quad (3.9)$$

where R_λ is the responsivity of the photodetector (measure of the optical-to-electrical conversion efficiency of the detector), P_1 and P_2 are the optical powers of the two fields, \vec{e}_1 and \vec{e}_2 their polarizations and φ_1 and φ_2 their phases. The photocurrent term at $|\omega_1 - \omega_2|$ is the beat signal, and can be measured if the difference $|\omega_1 - \omega_2|$ is smaller than the bandwidth of the photodetector, the beams are collinear $\vec{k}_1 = \vec{k}_2$ and the polarizations are not orthogonal $\vec{e}_1 \vec{e}_2 \neq 0$.

Therefore, instead of measuring directly the frequency spectrum of a phase-modulated light beam at optical frequencies, we can measure a 'beat spectrum', which is confirmed by the beat signals of the different bands from the phase-modulated field beating with an unmodulated optical field that has a slightly different frequency difference respect to the carrier frequency of the phase-modulated signal. If the difference in frequency of the unmodulated signal with the bands is smaller than the bandwidth of the photodetector then the 'beat spectrum' can be measured.

Given that P_m is the optical power of the phase-modulated wave, then the optical power content of one band is $P_k = P_m J_k^2(\beta)$ with $k = 0$ for the carrier band and $k = 1, 2, 3, \dots$, for the k^{th} pair of sidebands. Now, given that P_u is the optical power of the unmodulated wave that beats with the different bands, then the amplitude of one of the produced beat bands, according to 3.9, is proportional to $\sqrt{P_m J_k^2(\beta)}$. Therefore, the relative amplitudes of the beat bands are determined by $|J_k(\beta)|$ (and their power by $J_k^2(\beta)$). Knowing what is the relation between the amplitudes of the beat bands that we measure is essential for the method that we want to employ to determine the modulation index β . This is because the method relies on the fact that the relative amplitudes of the bands are determined ultimately by the value of the modulation index, which is true also for the beat bands that we measure.

3 Experimental setups and results

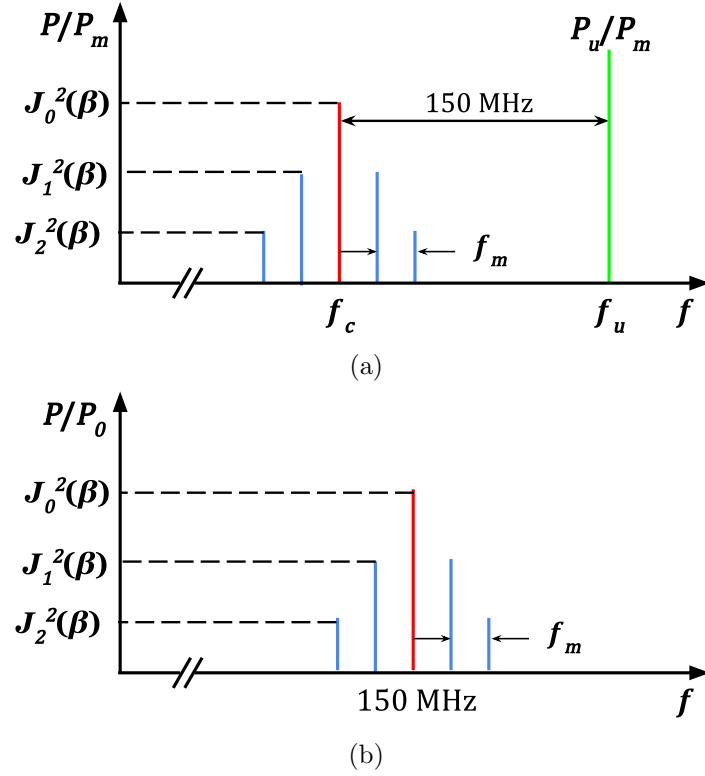


Figure 3.1: (a) Scheme of the frequency spectrum of bands from the phase-modulated wave and of the wave frequency-shifted by 150 MHz in terms of their power content (b) resulting spectrum of beat bands centered at 150 MHz

The setup presented in Figure 3.2 allows us to measure the frequency spectrum of the beat of a phase-modulated light with another light field frequency-shifted 150 MHz with respect to the carrier band. These beat signals oscillate with 150 MHz, $150 \text{ MHz} \pm f_m$, $150 \text{ MHz} \pm 2f_m, \dots$, –where f_m is the modulation frequency– thereby forming a frequency spectrum equivalent to that of the phase-modulated light field but centered at 150 MHz.

3 Experimental setups and results

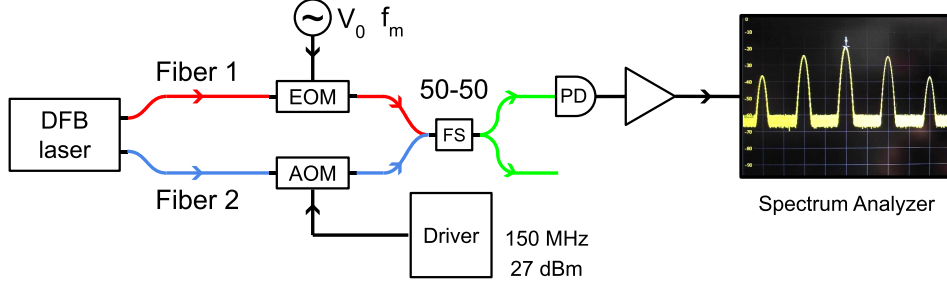


Figure 3.2: Scheme of the experimental setup used to measure the beat signal of a phase-modulate laser field with a single frequency laser light field. Two fibers with laser light from the same source (same frequency) are beat together. One of the beams is phase-modulated by the voltage-controlled EOM and the other is frequency shifted by 150 MHz from the carrier frequency of the phase-modulated beam using an AOM. The beams are superimposed using a Fiber Splitter (FS) and the beat signal is measured by a fast photodetector (PD) and amplified. The spectrum of beat bands is displayed by the Spectrum Analyzer.

Initially, two beams are separated from the same laser source: a Distributed Feedback Laser Diode (DFB), which is a tunable laser in the range 767-780 nm. The two outputs, at the same optical frequency ($\lambda \sim 780$ nm) are coupled into different optical fibers. One of the fibers (Fiber 1) is coupled to a Lithium Niobate electro-optic phase modulator (EOM) model NIR-MPX800-LN-0.1 supplied by iXblue. The light field undergoes phase-modulation after traveling through the EOM, which is controlled by a function generator that enables us to set the modulation frequency and the applied voltage (and hence the modulation index). The other light field, contained in Fiber 2, is frequency-shifted using a 780 nm Fiber Coupled Acousto-Optic Modulator (AOM) model T-M150-0.5C2W-3-F2S from the supplier Gooch & Housego. This device is externally controlled by a driver at a power of 27 dBm and a frequency of 150 MHz frequency and produces a frequency upshift also of 150 MHz on the light field of the beam 2. Then, both beams are overlapped using a 50-50 Fiber Splitter (FS) provided by Evanescence Optics, which takes 50% of power of each input beam and mixes them into two outputs, each of them with 50% of both beams. The Fiber Splitter provides the spatial overlapping required for the beat signal measurement. One of the fiber outputs of the Fiber Splitter, with an optical power of 3 mW is detected by a fast photodiode provided by Hamamatsu. The photocurrent measured by the photodiode is then amplified and analyzed by a Rohde & Schwartz HMS-X Spectrum Analyzer, which displays the frequency spectrum of the beat bands centered at 150 MHz.

To extract the value of β from the spectrum of beat bands displayed by the Spectrum Analyzer, we create a model consisting of peak functions (e.g. Gaussian or Lorentzian

3 Experimental setups and results

profiles) that represent the different beat bands. Thus, the functions are centered in the beat frequencies and their amplitudes are proportional to $J_k^2(\beta)$, different depending on the k^{th} beat band that they replicate. Fitting this model to the data from the Spectrum Analyzer implies that we find the value of β that provides the best amplitude relations between the functions so they suit the beat bands.

The Rhode & Schwartz HMS-x is a swept-tuned Spectrum Analyzer that displays the magnitude of the detected Fourier components (in this case the different bands) in terms of their power versus their frequency. These type of Spectrum Analyzers operate with bandpass filters, which are devices that pass certain frequencies and reject others. The frequency response of the filter expresses the gain that it provides (ratio of the output signal power to the input signal power) in terms of the frequency of the input signal. The function that determines the frequency response of the bandpass filter is known as the shape of the filter and the FWHM of this function is known as the bandwidth of the filter. The bandwidth of the bandpass filter used in the Spectrum Analyzer determines the spectral resolution of the instrument (the minimum bandwidth detectable by the instrument) and for this reason is called Resolution Bandwidth (RBW). If the bandwidth of the input signal to be analyzed is smaller than the bandwidth of the bandpass filter, then the spectrum of this signal will be displayed by the Spectrum Analyzer with the characteristic lineshape and bandwidth of the bandpass filter [24]. The HMS-X Spectrum Analyzer automatically sets a value of the RBW that allows a first measurement of the spectrum of an input signal. However, the RBW can be manually changed. This is relevant for the method that we use to obtain the value of the modulation index at different voltages since in this method we want to fit a model of functions that represent the spectrum of beat bands to the data points of the spectrum measured with the Spectrum Analyzer. With the automatic settings of RBW, the bands are displayed as almost single-frequency Fourier components. This is a good feature when we want to measure the frequencies of the bands but in this case it makes difficult the fit of any function to the profile of the bands. However, by setting a RBW bigger than the bandwidth of the input bands we can obtain an spectrum of bands displayed with a bigger bandwidth and the characteristic shape of the bandpass filter imprinted IN the bands, which is easier to modelize than shape of the near single-frequency bands. Furthermore, in this method the accuracy of the value of β depends on how good is the fit of the model of peak functions to the bands. For this reason, we want to have the maximum amount of data points forming the profiles of the beat bands because then the fit of a model function to a band will be more reliable. The Spectrum Analyzer provides 1000 data points along the span of frequencies displayed. The value of the span can also be changed manually. To obtain more data points forming the profile of the bands we can set the maximum value of the resolution bandwidth (RBW) which is 1 MHz because then, as we discussed previously, the width of the bands increases and more points are employed in forming the profile of the bands. On the other hand, we can reduce the span of frequencies to a situation where only 5 or 7 bands are displayed because this number of bands is enough to obtain the value of the modulation index from the fit.

3 Experimental setups and results

By reducing the span we also obtain more of the data points conforming the profile of the bands as it is shown in Figure 3.3.

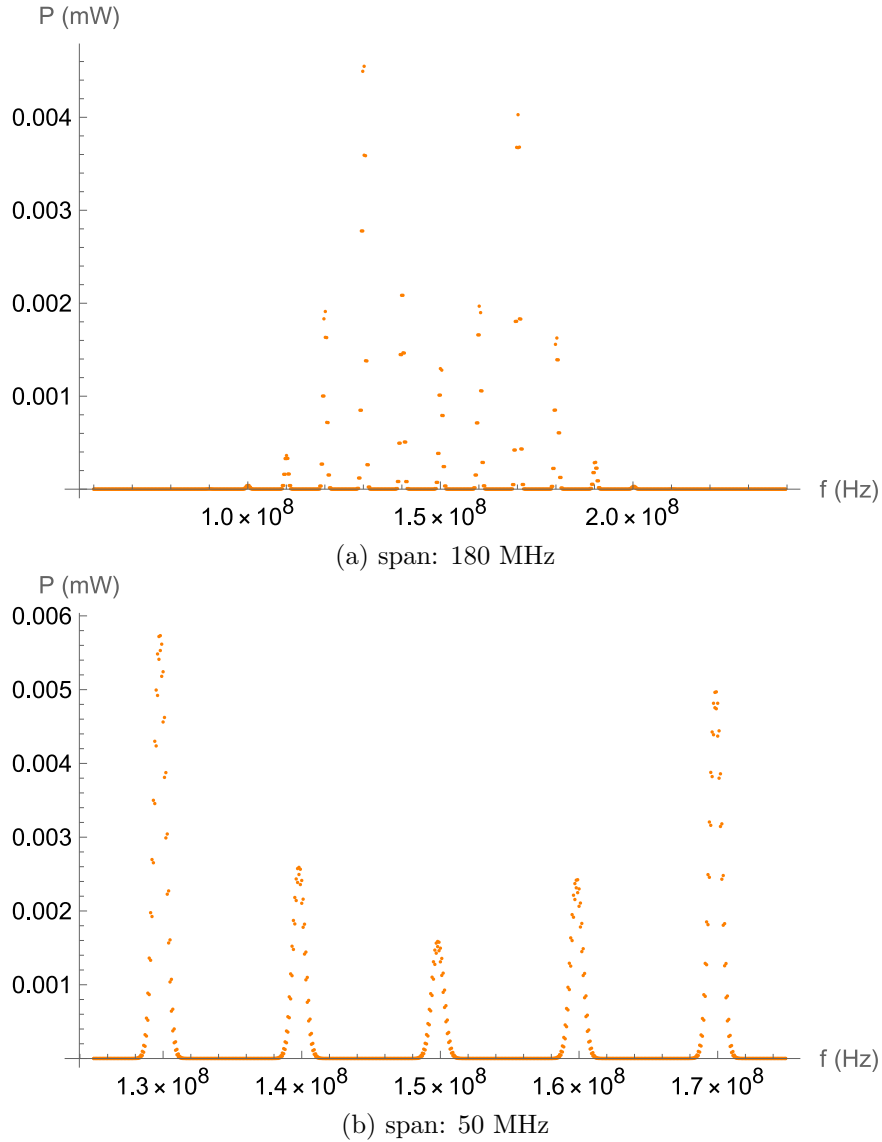


Figure 3.3: Data points of the spectrum of beat bands measured with the Spectrum Analyzer for a modulation frequency of 10 MHz and an input voltage in the EOM of 3 V (V_{pp}) using (a) 180 MHz span (b) 50 MHz span. In both cases the RBW is 1 MHz. Reducing the span we lose information about higher-order sidebands but in exchange the bands are defined by more data points.

3.1.3 Data treatment and results of the characterization of the relation modulation index versus applied voltage to the EOM

The setup presented in Figure 3.2 allows us to measure an spectrum of beat bands centered at 150 MHz. The Spectrum Analyzer displays the power of each beat band versus its frequency. This power is electrical power, so it is related to the beat bands' amplitude $i_{beat} \propto |J_k(\beta)|$ by $P_{beat} = i_{beat}^2 R$, being R the internal resistance of the Spectrum Analyzer. Hence, the relative magnitude of the beat bands displayed by the Spectrum Analyzer is determined by $J_k^2(\beta)$ which is the same characteristic of the power of the bands from a phase-modulated signal that we described in Section 2.6.1. We make use of this feature of the bands to extract the value of β from the beat spectrum. To do so, we construct a model of peak profiles (e.g. Gaussian or Lorentzian profiles) that imitate the different bands and fit this model to the data points measured with the Spectrum Analyzer. Therefore, in this model, for a certain modulation frequency f_m the functions are centered at the beat frequencies 150 MHz, $150 \text{ MHz} \pm f_m$, $150 \text{ MHz} \pm 3f_m, \dots$, and the peak value of this model functions is proportional $J_k^2(\beta)$ (for more details of the fit visit Appendix 5.1). After testing two different models, one where the bands are represented by Lorentzian functions and other where they are represented by Gaussian functions, we conclude that the model that best fits to the profile of the bands is the Gaussian model, as it can be seen in Figure 3.4, even though the values of the modulation index provided by both models are almost always the same. Another reason to choose the Gaussian model is that the error of the modulation index obtained is slightly smaller.

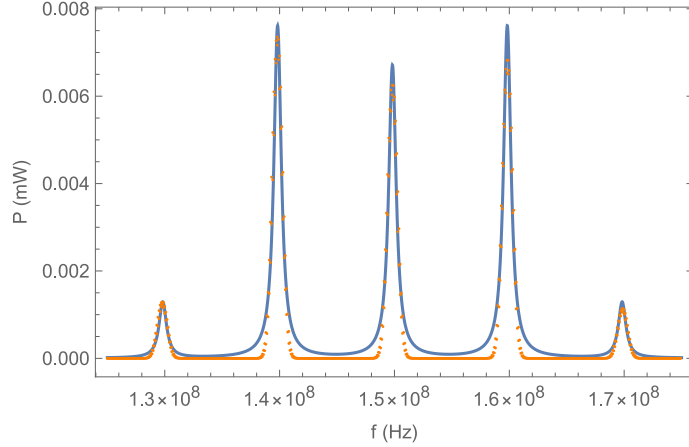
To characterize the relation modulation index versus applied voltage to the EOM for a given modulation frequency, we set in the function generator that controls the EOM a sinusoidal signal output with this modulation frequency and different values of the peak-to-peak voltage V_{pp} , which is related to the amplitude of the sinusoidal signal V_0 that appears in the expression (3.5) by $V_{pp}=2V_0$. For each values of V_{pp} we measure the spectrum of beat bands using the Spectrum Analyzer and then fit the Gaussian model to the data of the spectrum. As we explained before, to fit the Gaussian model to the spectrum of bands we reduce the span of frequencies displayed by the Spectrum Analyzer to a situation where they are measured only 5-7 bands in order to obtain more data points forming the profile of the bands. For this reason, we focus on measuring the spectrum when only the first two or three pairs of sidebands have a relevant amplitude, which corresponds to modulation indices $\beta < 2$. Proceeding like this, we obtain a set of points modulation index vs. voltage, that exhibit a linear behaviour as it is shown in Figure 3.5. With around 40 data points, we can fit a linear model, which is predicted by expression (3.5). In terms of the peak-to-peak voltage, the linear relation is

$$\beta = \frac{\pi}{2V_\pi} V_{pp} \quad (3.10)$$

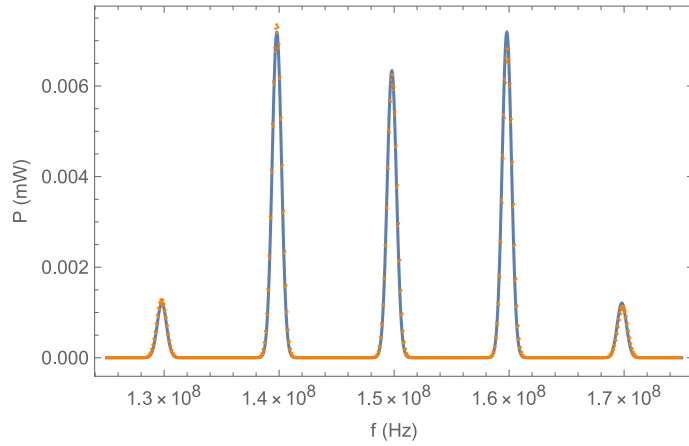
From the slope of this linear fit we extract the value of the parameter $\frac{\pi}{2V_\pi}$ that characterizes the relation β vs V_{pp} , and hence allows us to control the value of β for

3 Experimental setups and results

any applied V_{pp} to the EOM. Repeating the same procedure for different modulation frequencies we obtain slightly different dependencies, shown in Figure 3.6. We choose modulation frequencies around 10 MHz since it is an adequate value for generating an error signal in the Frequency Modulation Saturated Absorption Spectroscopy method.



(a) Model with Lorentzian functions. $\beta=1.483 \pm 0.003$



(b) Model with Gaussian functions. $\beta=1.483 \pm 0.005$

Figure 3.4: Data points (orange) of the spectrum of beat bands measured with the Spectrum Analyzer at 1 MHz RBW and 50 MHz span for a modulation frequency of 10 MHz and an input voltage in the EOM of 1.505 V (V_{pp}). In blue there are presented two different models for the fit to the beat bands (a) Model of Lorentzian beat bands. (b) Model of Gaussian beat bands. The value of the modulation index obtained is the same in both cases but the error is slightly bigger for the Lorentzian model (relative error of 0.3% versus 0.5%).

3 Experimental setups and results

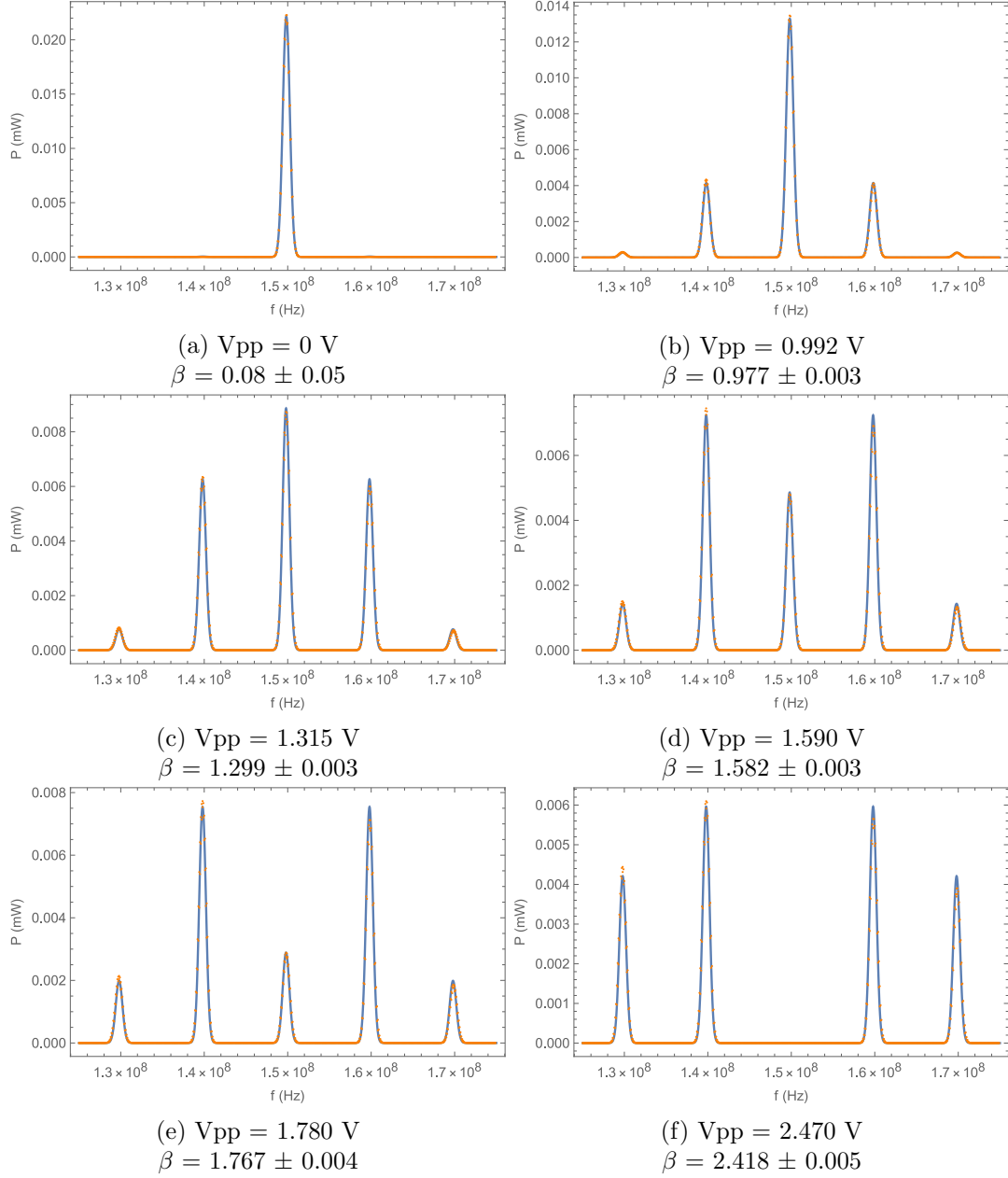
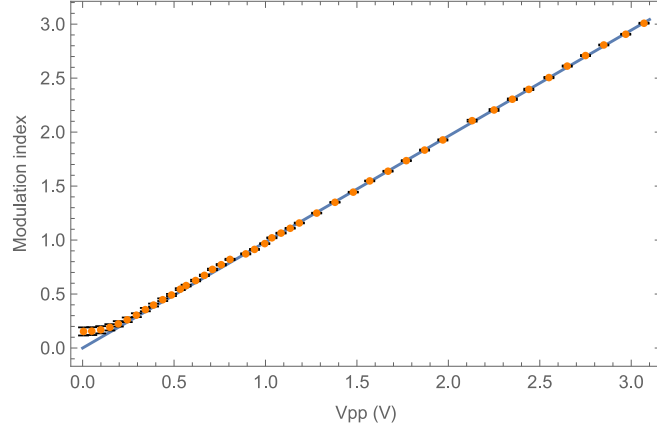
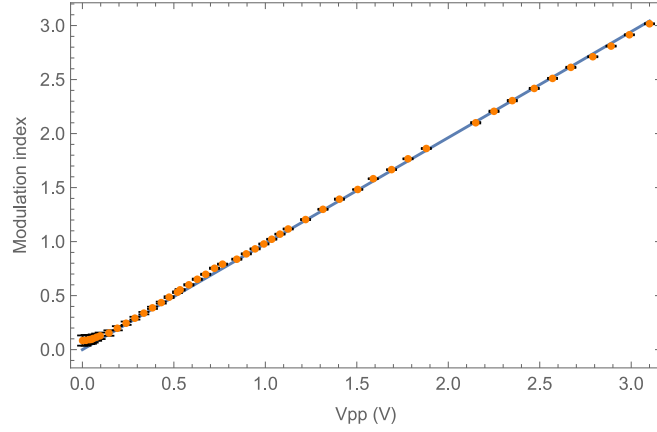


Figure 3.5: Plot of the model of Gaussian profiles (blue line) fitted to the data points (orange dots) measured with the Spectrum Analyzer for a fixed $f_m = 10$ MHz, and different peak-to-peak voltages V_{pp} applied to the EOM, presented with the resulting value of β from the fit. The settings of the Spectrum Analyzer are RBW: 1MHz, VBW: 10 kHz, SWT: 10 s and Span: 50 MHz

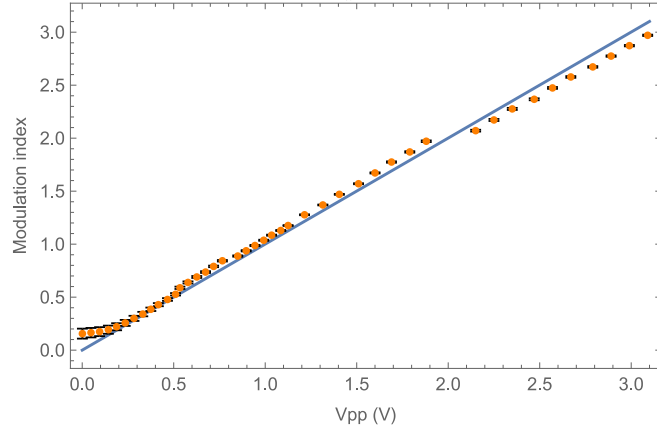
3 Experimental setups and results



(a) $f_m=5$ MHz, slope: $\frac{\pi}{2V_\pi} = 0.982 \pm 0.001 \text{ V}^{-1}$



(b) $f_m=10$ MHz, slope: $\frac{\pi}{2V_\pi} = 0.9812 \pm 0.0016 \text{ V}^{-1}$



(c) $f_m=15$ MHz, slope: $\frac{\pi}{2V_\pi} = 1.000 \pm 0.007 \text{ V}^{-1}$

Figure 3.6: Plot of the data points (orange) of the dependency β vs. V_{pp} for different f_m and linear fit (blue) applied to this data. The slope of the linear fit is identified with the parameter $\frac{\pi}{2V_\pi}$ that characterizes the relation modulation index vs. applied voltage to the EOM.

3 Experimental setups and results

Figure 3.6 shows that the relation between the modulation index and the applied voltage to the EOM is linear, as expected from the theoretical expression 3.5. This expression also predicts that the modulation index is zero for no applied voltage since there should be no modulation of the light when the EOM is not working. However, we can see in the graphs presented in Figure 3.6 that the values of the modulation index obtained from the fitted model do not tend to zero at small peak-to-peak voltages and therefore the points deviate from the linear behaviour. Even for 0 Vpp we obtain a non-zero modulation index, as we can see in Figure 3.5a. Furthermore, for these low voltages the error of the modulation index provided by the fitted model is also bigger as it can be seen in the error bars of the graphs. This can be explained from the fact that the peak values of the Gaussian functions of the model are given by $J_k^2(\beta)$ and for $\beta \rightarrow 0$ $J_0(\beta) \approx 1$ and $J_k(\beta) \approx 0$ for $k \neq 0$. Therefore, the noise floor from the spectrum displayed by the Spectrum Analyzer is interpreted by the fit as a non-zero amplitude of the sidebands, which leads to an also non-zero value of the modulation index. This occurs until the amplitude of the sidebands can be distinguished from the noise. We can also see in the graphs that there seem to be different linear regions. This is more noticeable in the graph 3.12c, where at 2 Vpp there is some sort of 'break' and after that threshold the slope of the linear dependency appears to be different. The reason behind is that there is a difference between the Vpp that we select manually in the function generator and the one that the device really displays. For instance, a selected value of 2 Vpp corresponds to ~ 1.88 Vpp when we measure it (e.g. using an oscilloscope) while a selected 2.1 Vpp corresponds to a measured value of ~ 2.15 Vpp. To solve this problem we measure the output Vpp voltage for every selected value in the function generator. However, the difference is still patent at different regions of voltage. We also must take into account that the fits are worse as we increase the modulation frequency, since that means that the span of the Spectrum Analyzer must be increased and therefore less data points form the profile of the bands.

We can now compare the value of the parameter $\frac{\beta}{V_{pp}} = \frac{\pi}{2V_\pi}$ obtained from the linear fits 3.6 to the estimation provided by the supplier company iXblue:

f_m (MHz)	$\frac{\pi}{2V_\pi}_{fit}$ (V^{-1})	$\frac{\pi}{2V_\pi}_{pred.}$ (V^{-1})	Discrepancy	Relative discrepancy
5	0.982 ± 0.001	1.006	0.024	2%
10	0.9812 ± 0.0016	0.993	0.0118	1%
15	1.000 ± 0.007	0.979	0.021	2%

Table 3.1: Comparison of the parameter $\frac{\pi}{2V_\pi}_{pred.}$ predicted by the relation given by the commercial supplier as a guideline with the slope of the linear fits presented at Figure 3.6 $\frac{\pi}{2V_\pi}_{fit}$.

As we can see in Table 3.1 the dependencies of the modulation index with the applied peak-to-peak voltage at the different modulation frequencies provided by the supplier are similar to the ones that we obtained from the fits, with a relative discrepancy

3 Experimental setups and results

$\sim 2\%$, calculated as $|\text{fit value} - \text{predicted value}|/\text{predicted value}$. However, the absolute discrepancies, calculated as $|\text{fit value} - \text{predicted value}|$ is not covered by the errors obtained from the linear fits. In fact, this error does not take into account systematic errors like the one we described regarding the voltage displayed by the function generator, which we can still notice in the graphs even after measuring the output peak-to-peak voltages. Other sources of error to be taken into account are possible systematic errors from the Spectrum Analyzer or the electronics. For example, in the fits of the Gaussian model presented in Figure 3.5, we can see that the sidebands of higher frequency than the carrier band have a visibly smaller magnitude than the sidebands with lower frequency than the carrier band. This can be due to a residual Amplitude Modulation at the modulation frequencies or due to some dependency of the electronics (e.g the amplifier) with the frequency. On the other hand, as we said before the predicted values are extrapolated from a measurement at $f_m=50$ kHz, while we use modulation frequencies three orders of magnitude bigger. For this reason we only use them as a reference to test the reliability of the experimental values.

To sum up, using this method we characterized the relation between modulation index β versus applied voltage to the EOM for different modulation frequencies f_m , which allows us to have control of the deviation frequency $\Delta f = \beta f_m$ of the equivalent Frequency Modulation of the light field produced by the EOM, and we are now able to investigate now the dependency of the SNR with the deviation frequency.

3.2 Investigation of the SNR dependency with the deviation frequency

With the characterization of the relation modulation index vs. applied voltage to the EOM presented in Section 2.1 we can control the deviation frequencies of the Frequency Modulation of the light field produced by the EOM. In Section 2.6 we presented the Frequency Modulation Saturated Absorption Spectroscopy method to generate an error signal with a transition frequency of Rb as frequency reference. At the same time, we also saw that the slope of the error signal, which is a measure of the signal-to-noise ratio is proportional to the deviation frequency. Therefore, we want to make use of the results obtained in Section 3.1.3 to investigate the dependency of the slope of the error signal with the deviation frequency. The interest behind is that a better laser frequency stabilization can be achieved with a higher signal-to-noise ratio. To do such an investigation, we need to generate and measure the error signal using the Frequency Modulation Saturated Absorption Spectroscopy method. In this Section we describe the setup that we used to put into practice this method and indicate which parts of this setup are integrated in the compact module. Finally, we present and discuss the results of the investigation of the dependency of the SNR with the deviation frequency for different combinations of modulation indices and modulation frequencies.

3.2.1 Setup for Saturated Absorption Spectroscopy

We perform Saturated Absorption Spectroscopy as part of the Frequency Modulation Saturated Absorption Spectroscopy method that we use to generate an error signal with a transition frequency of Rb as frequency reference. In Section 2.5 we described the working principle of this method, that requires two counterpropagating and overlapping laser beams at the same frequency that travel through an atomic gas—in this case Rubidium—. Measuring the intensity of one of the beams (probe beam) through the Rubidium sample we obtain the SAS signal $I_T(\nu)$ that presents resonant peaks when the frequency of the laser ν is tuned to one of the transition frequencies of Rubidium (see Figure 2.7).

The setup that we use to perform SAS is integrated into the compact module, as it can be seen in Figure 3.7b, and it includes waveplates or retarders, which are birefringent crystals capable to alter the polarization of the light that travels through them depending on the length and orientation of the crystal. Specifically we use a mounted Zero-Order Quarter-Wave Plate and a mounted Zero-Order Half-Wave Plate. We also use a 10 mm Polarizing Beam Splitter Cube PBS122 with wavelength range of 620-1000 nm provided by Thorlabs. This optical device transmits light with polarization aligned to its transmission axis and reflects light with polarization perpendicular to this axis. We also use a 12.7 mm diameter BK7 flat mirror provided by EKSMA Optics and mounted in a HVM-05i mirror mount provided by Newport. We also use a SM05PD1A reverse biased photodiode provided by Thorlabs that works with a recommended circuit provided by the manufacturer at a bias voltage of 5 V. All the optical elements are supported by mounts that leave them at the same height as the incoming beam, which is coupled into the SAS setup using a fiber coupler fixed with screws to one side of the module. At the same time all the mounts are screwed to the floor of the compact module using M4-screws to guarantee the maximum stability.

3 Experimental setups and results

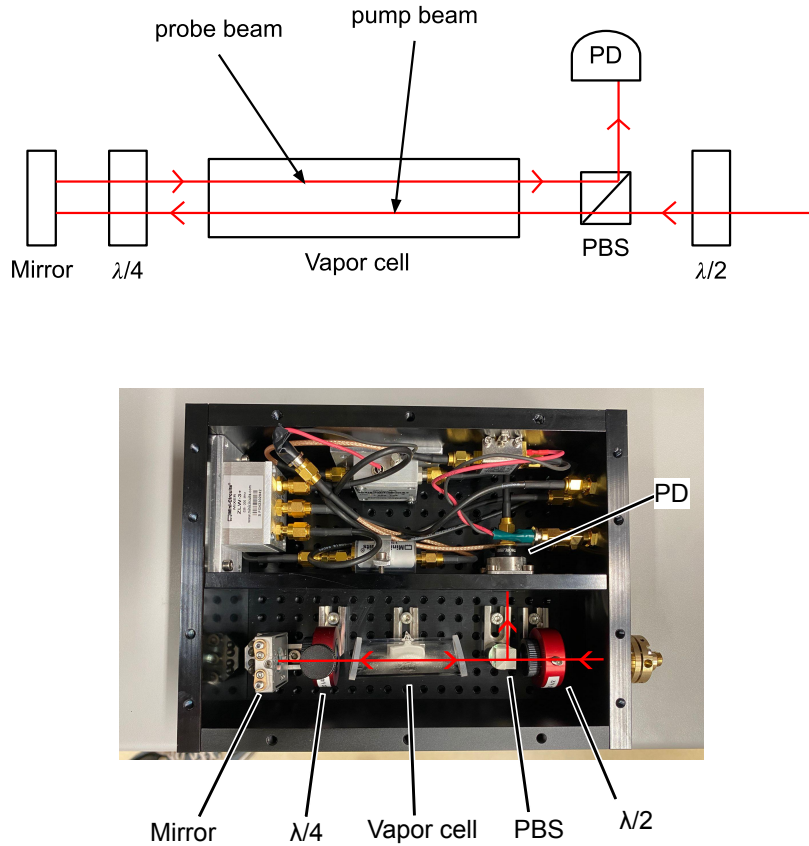


Figure 3.7: Scheme of the setup used to perform Saturated Absorption Spectroscopy and implementation in the compact module. The polarization of the incident pump beam is aligned to the transmission axis of the Polarizing Beam Splitter (PBS) using a half-wave plate ($\lambda/2$) and excites the atoms in the vapor cell. The beam is normally reflected in the mirror and acts as the probe beam (pump beam and probe beam are represented separated but they must overlap in order to interact with the same atoms). The quarter-wave plate ($\lambda/4$) is used to align the polarization of the probe beam with the reflection axis of the PBS, so it can be reflected in the PBS and measured by the photodiode (PD).

The incoming linearly polarized laser beam passes through a half-wave plate, which

3 Experimental setups and results

can rotate the linear polarization of the light by a certain angle depending on the relative orientation of the crystal and the incident polarization. The half-wave plate is used to align the polarization of the light with the transmission axis of the polarizing beam splitter (PBS). The alignment is evaluated by placing a powermeter after the PBS in the direction of the incoming beam (transmitted beam through the PBS) because the PBS transmits only the component of the polarization light aligned with its transmission axis and therefore the transmission will be maximum when both are aligned. The rotation of the polarization is performed by physically rotating the half-wave plate around the optical axis using the mount of the waveplate

After being transmitted through the PBS, the light beam, that acts as the pump beam, travels through the vapor cell containing the Rb atoms. Then, the beam passes through a quarter-wave plate and is reflected by the mirror. The power of the reflected beam is reduced compared to the pump beam due to the absorption from the Rb atoms in the vapor cell and now acts as a probe beam when it travels again through the vapor cell containing the Rb atoms. To make sure that the two beams overlap (necessary for the SAS method) we use the mount of the mirror that comes with driver adjusting screws which allow us to control the inclination of the mirror in the vertical and the horizontal direction. To make sure that the beam is normally reflected we use a small screen placed at some distance from the mirror in the direction of the reflected beam and then use the driver screws to adjust the direction until it overlaps with the incident beam.

The beam passes two times in total through the quarter-wave plate: one before being reflected and one after being reflected. The effect on the polarization of the light when the beam travels two times through a quarter-wave plate with the same orientation is equivalent to the effect produced by a half-wave plate. Therefore, function of this waveplate is also to rotate the polarization of the light to align it, this time, with the reflection axis of the PBS so it can be directed to the photodiode. To do so, we again evaluate the alignment of the light and the reflection axis of the PBS by placing the powermeter in the direction of the beam reflected by the PBS and rotating the quarter-wave plate until the power measured is maximum.

The intensity of the probe beam is measured by the photodetector and as the frequency of the laser is varied, the resonant peaks at the transition and crossover frequencies appear (see Figure 2.7).

3.2.2 Setup to generate and measure the error signal

The ultimate goal of the compact module that we build is that it is able to generate an error signal with one of the transition frequencies of Rb as frequency reference. To do so, according to the Frequency Modulation Saturated Absorption Spectroscopy method we need to incorporate to the SAS setup previously described, the EOM used to produce the Frequency Modulation of the laser light field that goes into the

3 Experimental setups and results

SAS stage and the electronic elements (mixer and low-pass filter) described in Section 2.6.2 to demodulate the AC error signal measured in this stage and hence obtain the DC error signal predicted by the expression (2.29). These electronic elements are integrated to the compact module, as shown in Figure 3.9, in addition to another element: the Bias Tee (BT). This is an electronic device capable of separating AC current from DC current. We use this device so we can obtain simultaneously two outputs from the compact module: one with the error signal and other with the SAS signal, which is useful to identify which error signal corresponds to which resonance frequency of the SAS signal. The setup 3.8 allows us to measure the generated error signal in an oscilloscope and it is also used in the investigation of the dependency of the SNR with the deviation frequency.

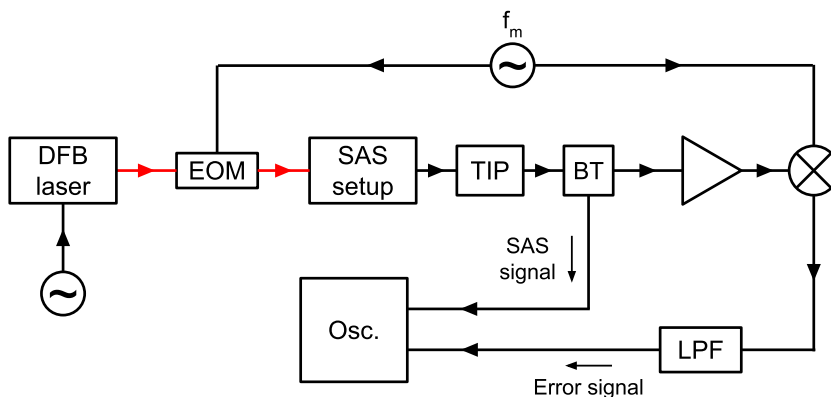


Figure 3.8: Scheme of the experimental setup used to measure in an oscilloscope the error signal and the SAS signal. The beam from the frequency-tunable DFB diode laser is modulated by the voltage-controlled EOM. Then the frequency-modulated beam is used to generate a FM SAS signal when passes through the SAS stage. This signal is amplified by the transimpedance amplifier (TIP) and then the Bias Tee separates the DC part, that corresponds to the SAS signal at the carrier frequency and the AC part which contains the error signal. The error signal is demodulated using the mixer and the low-pass filter to obtain a DC error signal. Both the SAS signal and the error signal are then measured in different channels of the Oscilloscope.

The laser source that we use the Frequency Modulation Saturated Absorption Spectroscopy method is again the DFB diode laser which a frequency-tunable laser in the wavelength range 767-780 nm. The optical power of the output laser beam is 1.75 mW. The frequency of the laser is controlled using a function generator, which allows us to span over time the transition frequencies of the D2 line of ^{85}Rb and ^{87}Rb with the laser frequency. The light field from the DFB laser source is modulated by the NIR-MPX800-LN-0.1 Electro-Optic Modulator from the company iXblue which we characterized in Section 3.1.3 and is voltage-controlled by another

3 Experimental setups and results

function generator that creates a sinusoidal signal. With the function generator we set the modulation frequency f_m and the peak-to-peak voltage, which corresponds to a modulation index β according to the characterization presented in Section 3.1.3. Therefore we set a known deviation frequency $\Delta f = f_m\beta$. The frequency-modulated beam then is used to perform SAS spectroscopy using the setup previously described in Section 3.2.1. The photocurrent measured in the SAS stage is amplified using the transimpedance amplifier (TIP). According to expression 2.23, this signal has an DC term that corresponds to the unmodulated SAS signal at the carrier frequency $I_T(\omega_c)$, and an AC term $\left. \frac{dI_T}{d\omega} \right|_{\omega_c} \cos \Omega t$ that is proportional to the error signal. Both terms are separated using a ZX85-12G-S+ Bias Tee. The DC term is directly measured by the Oscilloscope, providing the SAS signal described in Section 2.5. The AC signal is amplified using a ZFL-500+ Amplifier and is fed to a ZLW-3+ Mixer together with a sinusoidal signal from the same function generator that controls the EOM. Then this signal is filtered using an SLP-1.9+ Low-Pass Filter and providing the DC error signal that is also measured in another channel of the Oscilloscope.

The electronic components Bias Tee, Amplifier, Low-Pass Filter and Mixer, manufactured by Mini-Circuits, are incorporated in a compact way to the discriminant module and fixed to the walls of the module by screws and connected using SMA cables, as it is shown in Figure 3.9.

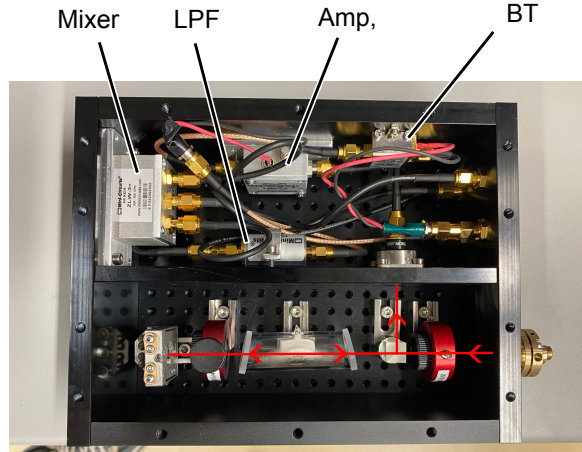


Figure 3.9: Picture of the electronic components ZX85-12G-S+ Bias Tee (BT), ZFL-500+ Amplifier (Amp.), SLP-1.9+ Low-Pass Filter (LPF) and ZLW-3+ Mixer integrated in the compact module.

3.2.3 Results of the investigation and discussion

As we stated in section 3.1, a better frequency stabilization can be achieved if the frequency deviations are measured with a high signal-to-noise ratio (SNR). This means that the discriminant provides large electric signals when there are small

3 Experimental setups and results

frequency deviations of the laser frequency to stabilized from the reference frequency. we also related the SNR to the slope of the error signal (V/Hz) provided by the discriminant. According to Section ??, the generated error signal in the FM SAS method is the derivative of a resonance of the SAS signal (approximately Lorentzian), that presents a linear regime near the resonant frequency. The slope of this linear regime (and hence the SNR), according to relation (2.26), is proportional to the amplitude of the error signal and at the same time the amplitude is proportional to the deviation frequency according to the expression (2.29). Therefore, bigger frequency deviations of the instantaneous laser frequency from its carrier frequency can lead to a higher signal-to-noise ratio. The aim of this Section is to investigate this dependency and determine the limits of this way of increasing the SNR.

To do this investigation we make use of the setup presented in Figure 2.10 that allows us to measure the error signal and the SAS signal in two different channels of the oscilloscope. We choose to investigate the crossover frequency of the ^{87}Rb D2 line $F_g=2$, shown in Figure ??. Instead of measuring directly how the slope varies with the deviation frequency we equivalently measure how the voltage difference between the maximum and minimum values of the error signal ΔV changes with the deviation frequency. To see this equivalency, we can consider the error signal ϵ in terms of the derivative of the Lorentzian resonance presented in Section ??.

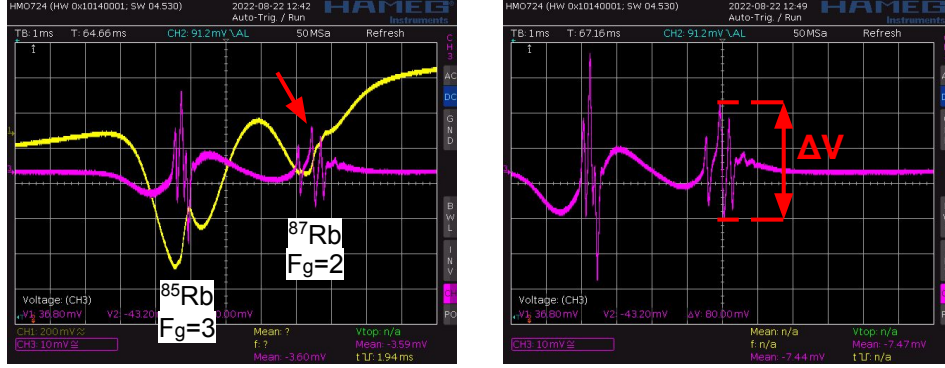
$$\epsilon(\omega) = \frac{1}{2}\Delta\omega \frac{dL}{d\omega} = \frac{-2I_0(\omega - \omega_0)/(\Gamma/2)^2}{\left[1 + \left(\frac{\omega - \omega_0}{\Gamma/2}\right)^2\right]^2} \quad (3.11)$$

being $\Delta\omega$ the deviation frequency, I_0 the amplitude of the Lorentzian, ω_0 the resonance frequency and Γ the FWHM of the Lorentzian. The position of the maximum and minimum values of the derivative are $\omega_{\pm} = \omega_0 \pm \frac{\sqrt{3}}{6}\Gamma$ and the quantity ΔV that we measure from the error signal in the Oscilloscope, in terms of the parameters of the Lorentzian is

$$\Delta V = \frac{1}{2}\Delta\omega \left[\frac{dL}{d\omega} \Big|_{\omega_-} - \frac{dL}{d\omega} \Big|_{\omega_+} \right] \quad (3.12)$$

which is proportional to the deviation frequency $\Delta\omega$ as well as the slope (see expression (2.26)), while the quantity $\frac{dL}{d\omega} \Big|_{\omega_-} - \frac{dL}{d\omega} \Big|_{\omega_+}$ only depends on the parameters of the Lorentzian (width center frequency etc.) and does not vary with the modulation frequency nor the frequency. The advantage of measuring this quantity is that it is extracted very easily using the markers tool of the Oscilloscope.

3 Experimental setups and results



(a)

(b)

Figure 3.10: (a) Screenshot of the Oscilloscope with the SAS signal displayed in one channel (yellow) and the error signal in other (purple). The error signal chosen for the investigation is pointed with a red arrow and corresponds to a crossover frequency of the D2 line of ^{87}Rb , as it can be seen from the comparison of the SAS signal with the one presented in Figure 2.7. (b) Representation of the ΔV parameter measured with the Oscilloscope.

To investigate the dependency of the ΔV parameter with the deviation frequency we choose one of the modulation frequencies for which we characterized the modulation index in Section 3.1.3. For this modulation frequency we vary the value of the modulation index by selecting different peak-to-peak voltages from 0 V to 3 V in the function generator that controls the EOM. The deviation frequency is given by $\Delta f = f_m \beta$. For every selected voltage and modulation frequency we measure the value ΔV of the error signal, providing a set of points ΔV versus Δf which are presented in Figure 3.12. The investigation of the dependency for a fixed $f_m = 15$ MHz presented at Figure 3.12c is perhaps the most relevant result, since we can see that there is a linear region like the one we described in the expression (3.12) but at a deviation frequency of $\Delta f \sim 15$ MHz the dependency starts to non-linear and the parameter ΔV starts to saturate. Visually, the error signal displayed by the Oscilloscope starts to show some asymmetry (see Figure 3.11) and therefore stops looking like the derivative of the resonance that we described in Section ???. This region of deviation frequencies is not explained by the theoretical model that we described. The reason of this could be that the condition that the condition of Δf small compared to the linewidth of the resonance that we used to derive the expression of the error signal as the derivative of the resonant signal is no longer fulfilled. The natural linewidth of the Rb D2 line transitions is ~ 6 MHz[?], but they must be added other possible sources of broadening such as pressure broadening and broadening derived from the SAS method (e.g the width of the SAS signal might increase with a bigger intensity of the pump beam). Therefore it seems reasonable to think that a deviation frequency of ~ 15 MHz is the limit of what we can consider small compared to the linewidth of the resonance in this

3 Experimental setups and results

case. For bigger deviation frequencies, even though the parameter ΔV of the error signal keeps increasing, we can no longer relate it to the slope of the error signal since the signal does not resemble the derivative of the Lorentzian anymore. The results for fixed values of f_m at 5 and 10 MHz presented in Figures 3.12a and 3.12b are similar to those obtained for a fixed f_m at 15 MHz with the difference that since the value of f_m is smaller, the values of $\Delta f = f_m \beta$ reached when we vary the modulation index from 0 to 3 are also smaller. Thereby, with $f_m = 5$ MHz we only reach a deviation frequency of ~ 15 MHz and therefore we only see the linear behaviour of the ΔV parameter with the deviation frequency, while for a fixed f_m at 10 MHz and values of the modulation index from 0 to 3 we reach a deviation frequency of ~ 30 MHz and therefore we get to see how the ΔV parameter from $\Delta f \sim 15$ MHz onwards starts to saturate and deviates from the linear behaviour. In the linear regions of the three graphs, the rate at which the ΔV parameter increases with the deviation frequency is ~ 2 V/MHz, being slightly bigger for a fixed f_m at 5 MHz, but this could be because the linear region is not spanned in its totality. In this graphs we can again see a break at a deviation frequency of $\Delta f \sim 20$ MHz for the graph of fixed $f_m = 5$ MHz and at $\Delta f \sim 30$ MHz for the graph of fixed $f_m = 15$ MHz. This break corresponds again to the systematic error of the function generator that controls the EOM, providing values of the peak-to-peak voltage that do not correspond to the ones selected.

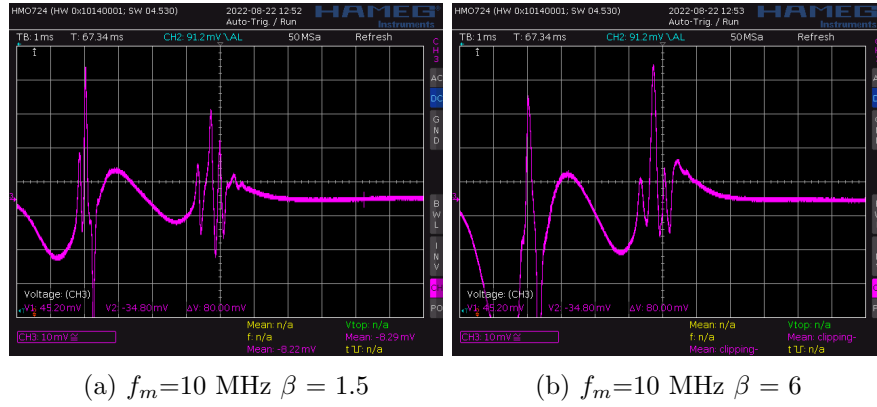
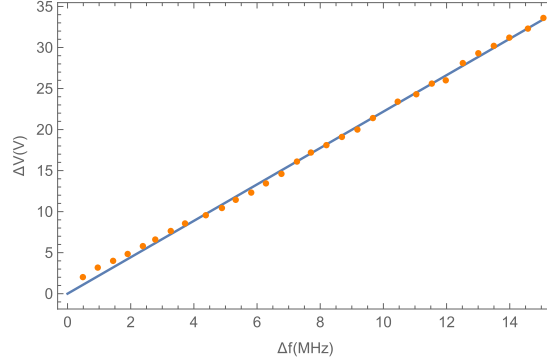
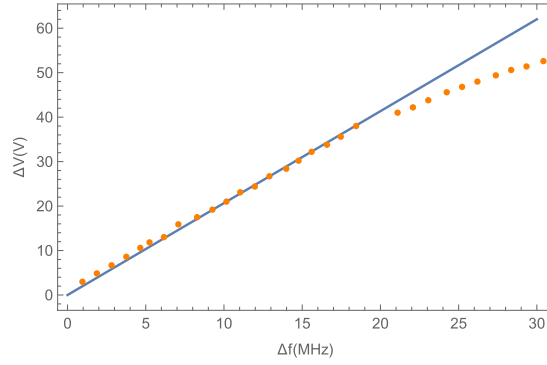


Figure 3.11: Comparison of two error signals with $f_m=10$ MHz and two different values of β (a) $\beta = 1.5$ (b) $\beta = 6$. For $\beta=6$ the error signal shows asymmetry and does not resemble the derivative of a Lorentzian, having a maximum value bigger than the minimum value.

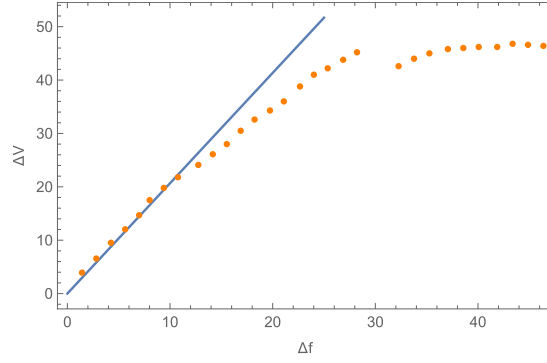
3 Experimental setups and results



(a) fixed $f_m=5$ MHz, slope in the linear regime: (2.22 ± 0.01) V/MHz



(b) fixed $f_m=10$ MHz, slope in the linear regime: (2.07 ± 0.01) V/MHz



(c) fixed $f_m=15$ MHz, slope in the linear regime: (2.07 ± 0.01) V/MHz

Figure 3.12: Dependency of the difference between the maximum and minimum values of the error signal with the deviation frequency $\Delta f = f_m \beta$. (a) Corresponds to a fixed $f_m = 5$ (b) Corresponds to a fixed $f_m = 10$ MHz (c) Corresponds to a fixed $f_m = 15$ MHz. The modulation index is varied for each fixed frequency providing different values of the deviation frequency. They are also presented linear fits (blue) at the regions where exists a linear behaviour predicted by the expression (3.12). The linear fits are realized using (a) all the data points (b) the first 20 points (c) the first 8 points. The slopes of the fits are presented together with their corresponding graph.

3 *Experimental setups and results*

The conclusion that we extract from this investigation is that as predicted with the theoretical model (3.12) there is indeed a linear dependency of the ΔV parameter –and hence the SNR– with the deviation frequency that we apply to frequency-modulated laser but this relation is limited to a certain region of deviation frequencies that might depend on the conditions of the experiment. For example a different laser power we might have obtained a different width for the resonances of the SAS signal and therefore the linear region could be different. On the other hand, we cannot affirm that using different combinations of modulation index and modulation frequency will lead to different linear relations, since even though we obtained a slightly better relation for a fixed f_m at 5 MHz, to do such an affirmation would have required to span the same region of deviations frequencies and with the same amount of points.

4 Summary and outlook

To summarize, in this thesis we were able to describe the construction of a compact discriminant module that can generate an error signal with one of the transition frequencies of Rubidium as frequency reference, putting into practice the technique of Frequency Modulation Saturated Absorption Spectroscopy described along Section 2. At the same time, we were able to characterize the dependency of the modulation index with the applied peak-to-peak voltage to the EOM at different modulation frequencies, which allows us to have control of the values of the deviation frequency applied to the light field at these modulation frequencies. Furthermore, we confirmed the validity of these results by comparing them with the theoretical estimations provided by the supplier company of the EOM iXblue and we also proposed possible sources of errors that would explain the small discrepancies between these results. Finally, thanks to this characterization we were able to study the dependency of the dependency of the signal-to-noise ratio of the signal generated by the compact discriminant module with the deviation frequency. In this investigation we could confirm the existence of a linear dependency region of the signal-to-noise ratio with the deviation frequency predicted by the Frequency Modulation Saturated Absorption Spectroscopy method. We also provided –for the experimental conditions described in Section 3.2.2– an approximated value of the deviation frequency that determines the end of this linear behaviour at $\Delta f \sim 15$ MHz. Finally, we also provided a possible explanation for this value related to the FM SAS method to generate an error signal as the derivative of a resonance, which was derived with the assumption of that the deviation frequency has to be small compared to the linewidth of the resonance which would also explain why the error signal starts to deform for values of the deviation frequency bigger than ~ 15 MHz.

Further steps in the investigation of the dependency of the signal-to-noise ratio with the deviation frequency could be to measure the linewidth of the resonance from which we generate the error signal because then we would be able to compare this value to the maximum deviation frequency value of the linear region. Another possible path in the investigation of how to improve the SNR of the error signal could be to test different powers of the laser light used in the FM SAS method and compare the slope of the different error signals at each power in order to find an optimal power. To conclude, one could also test the performance of the discriminant module in an Active Frequency Stabilization feedback-loop adding a Loop Filter (e.g. a PID controller) that stabilizes the tunable laser making use of the error signal provided by the compact discriminant that we constructed.

5 Appendix

5.1 Gaussian model of the bands of the spectrum of a phase-modulated signal

The fits of the Gaussian model of bands to the data of the spectrum of beat bands measured with the Spectrum Analyzer were performed using the function `NonLinearModelFit` of Wolfram Mathematica:

$$\text{NonlinearModelFit}[\text{fitdata}, \left\{ A \sum_{k=-2}^2 J_k(m)^2 \exp\left(-\frac{(f - f_0 - 10^7 k)^2}{2\Gamma^2}\right), m > 0 \right\}, \{m, A, \{\Gamma, 4 \cdot 10^5\}, \{f_0, 1.5 \cdot 10^8\}\}, f]$$

fitdata is a list with the data points power vs. frequency extracted from the Spectrum Analyzer, which can be imported directly from the .CSV file that contains the data using the function `Import`. The next element is the model to be fitted to the data. *A* is a generic amplitude for the bands, which are represented by the Gaussian functions $AJ_k(m)^2 \exp\left(-\frac{(f-f_0-10^7k)^2}{2\Gamma^2}\right)$, where *m* is the modulation index, *f* is the frequency and *f*₀ the central frequency of the spectrum (~150 MHz) and Γ the width of the Gaussian functions. As we can see from the sum, that goes from -2 to 2, in this example there are only being fitted two pairs of sidebands. This is because the span chosen in the Spectrum Analyzer only permitted to measure the first two pairs of sidebands. In this case the modulation frequency is 10 MHz, this can be seen from the center frequency of the different Gaussian functions, that are $f_0, f_0 \pm 10^7, f_0 \pm 2 \cdot 10^7$. The amplitude of each Gaussian function is proportional to $J_k(m)^2$. This is the key term that provides the value of the modulation index *m* from the fit since to fit the Gaussian functions to the measured spectrum requires to find the value of *m* that provides the best fit for all the Gaussian function as a whole. Here we also set the condition $m > 0$ since we don't get negative values of the modulation index by increasing the voltage of the EOM from 0 V_{pp}. The next terms grouped in a bracket after the model are the parameters to be fit. These are: the modulation index *m*, the general amplitude factor *A*, the width of the Gaussian functions which we set to be close to 0.4 MHz because it provides better fits $\{\Gamma, 4 \cdot 10^5\}$, the center frequency of the Spectrum, which set to be close to 150 MHz $\{f_0, 1.49810^8\}$ and finally the frequency *f* which is the variable of the Gaussian model.

Bibliography

- [1] H. Heylen et al. “High-resolution laser spectroscopy of $^{27-32}\text{Al}$ ” *Phys. Rev. C* 103, 014318 (2021)
- [2] B. E. A. Saleh, M. C. Teich “Fundamentals of Photonics” (2019) p. 599
- [3] QUANTUS projects, <https://quantus-projects.de/>
- [4] University of Bremen - QUANTUS IV - MAIUS, <https://www.zarm.uni-bremen.de/en/research/space-technologies/space-systems/projects/quantus-iv-maius.html>
- [5] W. Nagourey, “Quantum Electronics for Atomic Physics and Telecommunication” (2014) p. 323-374
- [6] B. E. A. Saleh, M. C. Teich “Fundamentals of Photonics” (2019) p. 563-567
- [7] B. E. A. Saleh, M. C. Teich “Fundamentals of Photonics” (2019) p. 583
- [8] D. A. Steck, “Rubidium 85 D Line Data” (2008, revised version 2021)
- [9] D. A. Steck, “Rubidium 87 D Line Data” (2001, revised version 2003)
- [10] G. Školnik, N. Vujić, T. Ban, “Optical pumping of the Zeeman components in the rubidium vapor” (2008)
- [11] B. E. A. Saleh, M. C. Teich “Fundamentals of Photonics” (2019) p. 584-586
- [12] B. E. A. Saleh, M. C. Teich “Fundamentals of Photonics” (2019) p. 593-596
- [13] J. Tatum “Stellar atmospheres”, Libre texts (2022) p. 182
- [14] D. W. Preston “Doppler-free saturated absorption: Laser spectroscopy” (1996)
- [15] B. E. A. Saleh, M. C. Teich “Fundamentals of Photonics” (2019) p. 645-651
- [16] S. Kraft et al. “Rubidium spectroscopy at 778–780 nm with a distributed feedback laser diode”, *Laser Physics Letters* 2 (2004) p. 71 - 76.
- [17] L. Der “Frequency Modulation (FM) tutorial” Silicon Laboratories Inc.
- [18] C. Finot, F. Chaussard, S. Boscolo, “Impact of a temporal sinusoidal phase modulation on the optical spectrum“ *European Journal of Physics*, European Physical Society, (2018) 39, pp.055303. [ff10.1088/1361-6404/aad61cff](https://doi.org/10.1088/1361-6404/aad61cff). [ffhal-01764502f](https://doi.org/10.1088/1361-6404/aad61cff)
- [19] G. C. Bjorklund, M. D. Levenson, W. Lenth, C. Ortiz, “Frequency Modulation (FM) Spectroscopy” *Appl. Phys. B* 32 (1983) p. 145-152
- [20] E. D. Black, “An introduction to Pound-Drever-Hall laser frequency stabilization” (2000)

Bibliography

- [21] W. Nagourey, "Quantum Electronics for Atomic Physics and Telecommunication" (2014) p. 52-70
- [22] B. E. A. Saleh, M. C. Teich "Fundamentals of Photonics" (2019) p. 977-980
- [23] RP-Photonics - Beat signal, https://www.rp-photonics.com/beat_note.html
- [24] "Keysight Spectrum Analyzer Basics Archived" Wayback Machine, p. 22,

6 Acknowledgement

I would like to thank Prof. Dr. Windpassinger for letting me do my Bachelor Thesis in the QOQI group and Prof. Dr. Pohl for accepting to be the second examiner of the thesis.

I would also like to thank André Wenzlawski for assisting me in any doubt I had and revising my thesis. In addition, I would like to thank the QOQI in general for making me feel very comfortable at the office.

Finally, I would like to give special thanks to Sören Boles for his mentoring. I learned a lot from him and I couldn't have done anything in the lab without his help.